# An investigation of the block shear strength of coped beams with a welded clip angles connection – Part II: Numerical study

Michael C. H. Yam[a*], Y. C. Zhong[b], Angus C. C. Lam[b] and V. P. Iu[b]

[a] *Department of Building & Real Estate, The Hong Kong Polytechnic University, Hung Hom, Kowloon, Hong Kong, China*
[b] *Department of Civil & Environmental Engineering, University of Macau, Macau, China*

**Abstract**

An experimental study of the block shear capacity of ten full-scale coped beams with a welded clip angles connection was presented in Part I. The test results were compared with predictions using block shear design equations in several current design standards. In general, the results showed that the existing design standards did not provide consistent predictions of the block shear capacity of coped beams with welded clip angles. In addition, the equations provided by the standards cannot accurately reflect the failure mode of the specimens observed in the tests. In order to gain a better understanding of the connection behavior, such as the stress distribution in the web near the periphery of the clip angles and the failure mechanism of the connection, an analytical study of the block shear capacity of coped beams with welded clip angles was carried out using the finite element method. Based on the limited test data and the results of the finite element analysis, a strength model was established and a design equation was proposed to evaluate the block shear strength of coped beams with welded clip angles. It was shown that the proposed design equation gave better predictions of the block shear capacity of the specimens.

*Keywords:* Block shear tests; Coped beams, Welded clip angles; Finite element analysis; General design guidelines

*Corresponding author: Tel. (852) 27664380; fax: (852) 27645131

Email address: bsmyam@polyu.edu.hk (Michael C. H. Yam)

## 1. Introduction

To investigate the block shear strength and behavior of coped beams with welded end connections, ten full-scale coped beam tests were conducted. Details of the results were presented in a companion paper (Yam *et al.*, [1]). In general, the failure mechanism in coped beams with welded end connections was different from that with bolted end connections since there was no reduction in the web section area due to bolt holes. The test results showed that only two of the ten specimens failed by block shear mode with tension fractures. Tension fractures occurred abruptly in the beam web underneath the clip angles. No shear fractures were observed and no tear-out type of block shear occurred. Local web buckling was also a potential failure mode for coped beams with welded end connections. High compressive stresses and shear stresses were localized in the web near the end of the cope due to a combination of bending and shear in the reduced section, hence resulting in extensive yielding at the cope and consequently inducing local web buckling. However, these specimens exhibited significant deformation of the block shear type prior to reaching their final failure mode.

In order to gain a better understanding of the failure mode of coped beams with a welded clip angle connection, a finite element analysis of all of the tested specimens was carried out. The results of the finite element analysis, such as the load deflection responses and the strain distributions in the beam web near the welded connection, were compared with the test results. Subsequently, a parametric study was conducted by using the validated finite element model. The parameters included the effect of the aspect ratio of the clip angle, the shear and tension areas, web thickness, cope length, cope depth, connection position, and the rotational stiffness of the clip angles.

## 2. Finite element analysis of the test specimens

### *2.1 Finite element model*

Ten three-dimensional nonlinear finite element models corresponding to the test specimens were established in ABAQUS 6.3 [2]. Both the material and geometric nonlinearities were considered. Measured dimensions of the test specimens were used for the models in order to accurately represent the geometries of the beam and the welded clip angles. Four-node, reduced integration, and finite strain shell elements (S4R, the general purpose shell element in ABAQUS) were used to model the entire coped beam, including the beam web, the flanges, and the stiffeners. The double clip angles were discretized using eight-node linear incompatible brick elements (C3D8I). Round bolt holes were also modeled in the outstanding legs of the double clip angles. These elements are capable of representing large deformations, and geometric and material nonlinearities, and provide robust and accurate solutions to most applications. The representative finite element mesh is shown in Fig. 1 (a).

Another important question to be addressed in the simulation was the fillet welds that connected the beam web and the double clip angles. In fact, the actual weld sizes for the test specimens were relatively large. It was found that the weld group was compact and that the welds did not fail during the test. Thus, it was assumed that negligible weld deformation occurred during the test. Hence, rigid links were used between the web of the beam and the angles in the models to simulate the effects of weld. The rigid links constrained all degrees of freedom of the corresponding nodes of two connected parts. In ABAQUS, BEAM constraints of the multi-point constraints (MPC) type were used for this purpose. They provided a rigid link between two nodes to constrain the displacement and rotation at the first node to the displacement and

rotation at the second node, corresponding to the presence of a rigid beam between the two nodes. As far as the model was concerned, there were two groups of MPC BEAM elements along the connected path. The inside ones linked the edge of the angle to the beam web straightly at the weld root and, the others linked the centerline of the thickness of the angle to the beam web at the weld leg so as to be consistent with the measured weld sizes. The arrangements are illustrated in Figs. 1(b) and 1(c). It should be noted that the contacts between the web of the beam and the double clip angles were neglected.

Boundary conditions were modeled to accurately represent the supporting conditions of the experiments. For the test specimens, roller assemblies were used at the load position and at the support so that both rotations and longitudinal movements were allowed. In addition, washers were placed between the outstanding leg of the angles and the flange of the supporting column to provide clearance and minimize the end rotational stiffness of the connection. Therefore, a simply supported condition could be assumed for the test specimen. To model the supported end of the beam, the vertical translation degrees of freedom (DOF) at the bottom beam edge were constrained ($U_2$ = 0), as shown in Fig. 1 (c).

Since there was no contact between the angle plates and the column flange, the boundary condition for the double clip angles could simply be imposed at the nodes around the bolt holes of the outstanding leg. Then, the vertical and out-of-plane displacements around the bolt holes at the outstanding angle legs were constrained ($U_2$ = 0, $U_3$ = 0). In addition, as could be observed from the tests, there was a slight rotation of the clip angles due to the bolt deformation as the load was applied. In order to simulate the deformation of the snug-tight bolts, bilinear SPRING1 elements were used between the clip angles and the column flange, acting in the horizontal direction (1-

direction) to allow a slight flexible rotation. There were a total of about 200 SPRING1 elements at the nodes around the bolt holes. The tensile and compressive stiffness of the spring was 200 N/mm at the first 0.5 mm. Beyond this limit, the stiffness was changed to a relatively large value of 40000 N/mm per spring. The boundary conditions of the connection are schematically shown in Figs. 1(b) and 1(c). The determination of these values and the effects of the spring stiffness will be discussed in the parametric study presented later.

Lateral bracings were provided at both the load position and the support to prevent lateral movement of the test beam. Therefore, in the model, lateral supports (bracings) were imposed at the flanges of these two positions: one near the load point and the other at the supported end ($U_3 = 0$). The load was increased vertically at the load point, as shown in Fig. 1(a). In addition, to analyze the problem of instability, it was necessary to introduce an initial imperfection into the "perfect" geometry of the model. In fact, in the experiments nearly all of the specimens buckled to some extent in the same direction near the cope ends. Thus, it was reasonable to assume a loading imperfection at the load position due to possible load eccentricity or slight load tilting, which was hard to avoid in the test setup. To introduce this loading imperfection to the FE model in a simple way, a small lateral load was added at the load point to initiate the expected instability. The magnitude of this lateral load must be sufficiently small so that it does not affect the overall solution. For all models, the lateral loading imperfection was chosen to be 2% of the vertical applied load, imposed at the load point where it was 50 mm away from the existing lateral bracings.

### *2.2 Material Model*

The isotropic elastic-plastic material properties with the von Mises yield criterion were employed for the finite element analyses to represent the material

nonlinearities. Data on the static strength of the material were gathered from the tension coupons of the associated test beam webs. The nominal stress ($\sigma_{nom}$) and nominal strain ($\varepsilon_{nom}$) in the static curve evaluated from the tension coupon tests were then converted into the true stress ($\sigma_{true}$) and true plastic strain ($\varepsilon^{p}_{true}$) for the input to ABAQUS, by using the following equations:

$$\sigma_{true} = \sigma_{nom}\left(1+\varepsilon_{nom}\right) \tag{1}$$

$$\varepsilon^{p}_{true} = ln\left(1+\varepsilon_{nom}\right) - \left(\frac{\sigma_{true}}{E}\right) \tag{2}$$

It is known that substantial localized deformation continues to develop in a tension coupon after reaching the ultimate load and before the specimen eventually breaks. At this stage the stress and strain are no longer calculated based on the initial dimension. In order to obtain reasonable material properties after necking, a material stiffness after peak load was assumed. Based on the study by Khoo *et al.* [3] and for the purpose of being conservative, a post-ultimate stiffness of 200 MPa was assumed, and the material true plastic strain was extrapolated linearly to 1.0. The material was assumed to be perfectly plastic beyond a true plastic strain of 1.0.

A summary of the parameters for the material model for Beam A to E and the clip angles are given in Table 1, as the input values for ABAQUS. In addition, by taking the average of the measured data of all tension coupons from the test beams, a general material model was obtained and was also included in the table. The typical true stress versus the true plastic strain curve can be found in Fig. 2. This general material model is used for the analyses in the parametric study that will be presented later.

### *2.3 Procedures for the analysis*

In order to determine the nonlinear load deflection curve of the test beam and the behavior of the descending branch of the curve, a modified Riks method was utilized in the analysis. Load control was used in the initial portion of the load displacement response and displacement control was used subsequently to capture the nonlinear part of the curve and the maximum load. The analysis was terminated when excessive out-of-plane movement occurred in the web, which corresponded to a 10 mm lateral displacement at a monitoring point in the beam web near the end of the cope. To predict the tension fracture failure for block shear, a strain-based failure criterion, which was adopted by Cheng *et al.* [4], was used. In this criterion, failure was assumed to have occurred when the maximum strain reached a critical value. For the current models, the critical equivalent plastic strain (PEEQ) was assumed to be 0.2, which was calibrated from the test results. Consequently, if the maximum PEEQ of the beam web located at the area of tension underneath the clip angles reached 0.2, the material was assumed to have failed by fracture. The corresponding fracture load was therefore captured.

## 3 Finite Element Analysis Results

### *3.1 General*

Generally, similar behavior was observed in all of the analyses. The analytical results showed that linear load deflection behavior occurred in the initial stage of loading. When nonlinear behavior commenced, yielding first appeared in the beam web underneath the welded clip angles or near the cope end. Flexural stresses as well as shear stresses in the vertical plane near the welded angles caused early yielding in the web plate near the cope end. As the load increased, the web plate in this region distorted or buckled inelastically. Subsequently, the load descended due to the excessive local web buckling. For some models, significant elongation of the web material underneath

the welded clip angles was observed. The maximum PEEQ was found at the outer beam end underneath the welded clip angles. When this PEEQ reached the critical value of 0.2, the model was regarded as having failed by block shear with tension fractures. In general, the results of the analysis matched well with the experimental findings that the test specimens that failed by block shear had their tension failure at the outer end of beam web underneath the welded clip angles. On the other hand, for the other models, severe compression as well as shearing resulted in local web buckling at the cope end. In addition, for these models there was less elongation in the area of the web underneath the clip angle.

The typical deformed shapes of the model connection are shown in Fig. 3. The von Mises stress contours and the equivalent plastic strain contours of model D1 for the last load step before ultimate failure are shown in Fig. 4. As shown in these figures, there were high stresses and significant plastic deformation at two critical regions, indicating that failure would occur either in the beam web underneath the clip angles or near the cope end. Generally, it can be found that tensile stresses in the tension area underneath the clip angles reached the ultimate strength of the material, while yielding had developed along the shear area near the clip angles. In fact, the highest plastic strain occurred in the web right underneath the end of the clip angles where material fractures would occur as shown in Fig. 4.

### *3.2 Load deflection behavior*

The analytical load deflection curves of two typical models (one that failed in the web buckling mode and the other that failed in the fracture mode) were compared with the curves obtained from the experiments, as shown in Fig 5. The analytical load deflection curves for the other specimens can be found in Zhong *et al.* [5]. The analytical and the test results of all of the specimens are summarized in Table 2.

It can be seen from the figures that the load deflection curves obtained by the analysis were in good agreement with those of the test results. In most cases, the analyses could trace the entire load deflection curves and provide good matches. The average value of the ratio of the test capacity to the analytical prediction was 1.04 and 0.98 for the block shear cases and the local web buckling cases, respectively. In addition, as shown in Table 2, among the eight specimens that reached their ultimate loads, the finite element models could accurately predict the failure mode for seven of them. The discrepancy in specimen D1-457R1 might be due to the insufficient restraints provided by lateral bracing during testing, as described in the companion paper (Yam *et al.* [1]). As can be seen from the test results of this specimen, severe web necking was observed in the area of tension underneath the clip angles, implying that tension fractures would probably occur as predicted. In addition, the analyses also provided the failure mode predictions for specimens C1-457R3 and D2-457L, showing that tension fractures would probably occur at a higher load if the capacity of the loading frame were higher.

### *3.3 Strain distribution*

In order to confirm the validity of the finite element model simulations, the strain distributions at critical areas around the web block were also examined. For simplicity, only the analytical strain distributions along with the test results for specimen E1, as shown in Figs. 6 to 8, are discussed. The analytical results for the other specimens can be found in Zhong *et al.* [5]. These figures illustrate the tensile strain distributions along the horizontal plane (the tension area), the bending strain distributions, and the shear strain distributions along the vertical plane (the shear area), respectively.

The vertical longitudinal strain distributions at the strain gauge locations along the area of tension with two levels of load are shown in Fig. 6. It can be seen that the analytical result provides a good prediction of the strain distribution obtained experimentally by the strain gauges. The situation is similar in the case of bending strain (in the horizontal direction) distributions along the vertical plane, as shown in Fig. 7. As to the shear strain distributions along the shear area near the welded clip angles, more analytical data were collected in this area so that the entire distribution could be presented as shown in Fig. 8. As indicated in the figure, the shear stress distributions exhibit slight jumps near the corners of the clip angles. This was due to the influence of concentrations of stress around the corners of the welded clip angles. Hence, it was difficult to make a direct comparison of the shear strain readings measured by the top and bottom rosettes near the angle corners. However, reasonable agreement is still obtained between the predicted values and the limited measured data.

In general, the strain distributions of other specimens are similar. It is therefore concluded that strain distributions at the critical areas can be well simulated within the elastic stage by the current finite element models. It is also believed that the strain or stress distributions at higher loads can also be predicted by the models. Nevertheless, the finite element models are capable of not only predicting failure capacities but also of tracing the entire load versus the deflection curves.

### *3.4 Stress distribution*

As illustrated in Fig. 9, a typical tensile stress distribution was plotted on the horizontal plane A, while a shear stress distribution was plotted on the vertical plane B for specimen E1-356T. The planes were located at a distance of 10 mm away from the edge of the fillet welds around the clip angles in order to avoid the effects of

concentrations of stress at the weld edge. The stresses at both the elastic stage and the ultimate failure stage were plotted in same figure for purposes of comparison. The applied load level was chosen to be 183 kN for the elastic stage and 702 kN for the ultimate failure stage, respectively. It can be seen that, at the elastic stage, the tensile stress distribution on the horizontal plane was triangular, and the stress was largest at the beam end and decreased along the area of tension. The shear stresses along the vertical plane exhibited a slight jump near the corners of the clip angles due to concentrations of stress at these positions. Subsequently, when the connection failed due to block shear with tension fractures, identified by critical value of the PEEQ, the tensile stress distribution became a parabolic curve. This profile could also be assumed to be a trapezoid approximately along the area of tension. It was also observed that higher tensile stresses were present towards the end of the beam web. When the ultimate strength of the material was reached, the beam web underneath the clip angles began to neck.

As to the shear stress distribution at the ultimate stage for specimen E1-356T, the shear stress increased linearly from zero at the top edge of the beam web and reached an approximately uniform distribution in the web along a vertical plane between the top and the bottom corners of the clip angle, as shown in Fig. 9. Moreover, it was found that the maximum shear stress of the uniform portion was less than the shear fracture strength of the material. Hence, this substantiated the view that no shear fracture had occurred along the vertical plane.

## 4. Parametric Study

### *4.1 Description of the geometry of models and modeling techniques*

To provide a better understanding of the block shear behavior of coped beams with a welded clip angles connection and to identify important parameters that may influence the connection strength, a parametric study was conducted. Based on the test results and the analytical results of the test specimens, four groups of parameters were chosen in this study. The parameters included: (1) the aspect ratio of the clip angle, (2) the shear and tension areas, (3) the cope length, cope depth, and connection position, and (4) the rotational stiffness of the clip angles.

The parameters and the variables considered are summarized in Table 3. Finite element models were developed and analyzed using ABAQUS, as described previously. Two beam sections, UB356 (Beam356) and UB457 (Beam457) (SCI, [6]), were chosen for the finite element analysis. The span of the beams was 3.3 m and the thickness of the clip angles was 16 mm, which was the same as those used in the experimental program. The dimensions of the beam and the connection details are shown in Table 3. It should be noted that the cope dimensions were fixed for all of the models, unless stated otherwise. The cope length in each model was kept at a constant distance of 50 mm extending from the end of the angles (i.e. $c = a$+50 mm), except for the models that were employed to compare the effects of cope length. More details of the models can be found in the footnotes to Table 3.

As was shown before, the simulation results of the finite element analyses for the test specimens were in close agreement with test results. Therefore, the same technique was employed to develop the finite element models of the coped beam specimens in the parametric study. For the material properties, a general isotropic elastic-plastic material property (Table 1) was used for all of the models. The true stress-true strain curve was obtained by taking the average of the measured data of all tension coupons from the test beams with the yield strength ($F_y$) and ultimate strength

($F_u$) being 320 MPa and 460 MPa, respectively. In addition, the elastic modulus (E) and the Poisson's ratio (ν) used in the study were 205000 MPa and 0.3, respectively. The critical PEEQ was assumed to be 0.2, since this value has been verified to be a reasonable value in a previous calibration in a finite element analysis of the test specimens. If the maximum PEEQ of the beam web at the area of tension underneath the clip angles reached 0.2, tension fracture failure in this area was assumed to have occurred.

## 5. Results and discussion of the results of the finite element parametric study

### *5.1 Effect of aspect ratio*

For the series of aspect ratio models, the design capacities of the related connections were nearly identical for the purpose of comparison. In order to reveal the representative results, the analyses for the effects of aspect ratio were carried out on two beam series, i.e. Beam356 and Beam457, respectively. The aspect ratio was varied from 1.4 to 4.8. with a simultaneous increase in shear area and decrease in tension area, where the shape of the connection changed from short and wide to tall and narrow. Figure 10 shows that the connection capacity increased as the aspect ratio increased. However, for a large aspect ratio, a small increase in the capacity of the connection was observed. In particular, for the models of Beam356, the capacity did not increase when the ratio was varied from 2.3 to 3.6. This indicated that the capacity of the connection with local web buckling failure mode would not be significantly improved by an increase in the aspect ratio. Besides, when the aspect ratio increased, the local web buckling failure mode tended to occur. This could be observed from the models of Beam457 and Beam356, with beam web thicknesses of 7.6 mm and 9.1 mm,

respectively. For models with thinner web (web thickness less than or equal to 7.0 mm), local web buckling failure was observed.

Based on the results of the test and of the finite element analysis, it was believed that increasing the shear area would have more pronounced effect on the connection capacity than increasing the tension area. In order to reveal this relationship and develop a better prediction equation for connection capacity, the shear area and the tension area were investigated. The findings will be presented in the following section.

### *5.2 Effect of shear and tension areas*

The effect of shear area was investigated by keeping the tension area constant and varying the shear area in the connection. Figure 11 shows that the capacity of the connections improved by increasing the shear area. It can be seen that a 20.3% and 16.4% increase in capacity was achieved when the shear area was varied from 120 mm to 160 mm, with *a* equal to 50 mm or 70 mm, respectively. However, the rate of the increase indicated that where the shear area was larger, less of an improvement in capacity was seen. Only a 4.4% increase in capacity was found when *b* was varied from 160 mm to 200 mm, with *a* equal to 50 mm. Nevertheless, a larger shear area could lead to greater resistance of vertical force and contribute to the strength of the connection. In addition, it was observed that a larger shear area would lead to the local web buckling failure mode instead of to tension fractures. This might be due to the fact that more vertical force was carried by the larger shear area; therefore, the stress and deformation of the tension area were insufficient to allow tension fractures to occur. In addition, for the same connection capacity, an increase in the shear area would lead to a corresponding decrease in the tension area; hence, the connection eccentricity was reduced. As discussed in the companion paper (Yam *et al.* [1]), the connection

eccentricity induced high compressive stress in the web between the clip angles and the cope end, initiating local web buckling of the connection.

Similarly, the effect of tension area was investigated by keeping the shear area constant and varying the tension area. It should be noted that two analysis cases associated with details of the cope length were considered. First, in Case A, the distance between the cope end and the clip angles was given a constant value of 50 mm. In other words, the cope length was extended 50 mm away from the end of the clip angles (i.e., $c = a+50$ mm). For example, when the length of the tension area $a$ was 50 mm, the cope length $c$ was 100 mm; similarly, when $a$ was 100 mm, $c$ was increased to 150 mm. It was found that the capacity did not significantly improve when the tension area was increased in such models as shown in Fig. 12 (a). On the contrary, increasing the area of tension resulted in a slight reduction in capacity for the $b$=160 mm cases. Local web buckling tended to occur when the area of tension was increased with a larger cope length. Second, in order to eliminate the influence of different applied bending moments at the cope end due to varying cope lengths, additional analyses on identical cope lengths were carried out as Case B. The results are shown in Fig. 12 (b). For the models in Case B, the connection configurations were similar to those of Case A, except that the cope length ($c$) was kept at a constant value of 100 mm. As shown in Fig. 12 (b), by increasing the area of tension, the block shear capacity with tension fractures increased almost linearly. However, only an improvement in capacity of 8.6% and 7.2% was achieved when $a$ was varied from 50 mm to 100 mm ($b$=160 mm) and from 50 mm to 90 mm ($b$=120 mm), respectively. Compared with the shear area effect, the influence of the tension area on the connection capacity was less pronounced than that of the shear area. This also validated the results in the aspect ratio study showing that an increase in

shear area had more pronounced effect on the connection capacity than a decrease in tension area.

In conclusion, the results of both Case A and Case B indicated that increasing the tension area would not lead to a significant increase in connection capacity. It was believed that a large area of tension would increase loading eccentricity and hence generate more bending moments to the edge of the beam web region near the clip angles.

### *5.3 Effect of cope length, cope depth, and connection position*

The cope length ($c$) measured from the beam end was varied between 0 mm and 200 mm in 50 mm increments in the parametric study. The analyses were conducted based on three different thicknesses of beam web of Beam457, with identical connection dimensions ($a$=50 mm and $b$=120 mm). With regard to the details of the connection used in the study, most models failed due to tension fractures. The analytical results show that connection capacity decreased as cope length increased, as shown in Fig. 13. The figure also shows that there was a significant decrease in block shear capacity when the cope length increased from 50 mm to 100 mm. When the cope length of the connection increased from 100 mm to 200 mm, a reduction in block shear capacity of only about 6% was obtained for the cases of tension fracture. For a small cope length (for example, $c$ = 0 mm to $c$ = 50 mm) the uncoped part of the top flange covered the shear path region of the web block; hence, the connection was strengthened because the top flange could carry a portion of the shear force. Local web buckling could also be prevented in such cases due to the stiffening effect of the top flange. Nevertheless, a large cope length would increase the possibility of web instability and induce local web

buckling failure. In addition, increasing the cope length would directly increase the applied bending moments to the cope end, and thus decrease the connection capacity.

For the models of the cope depth series, the cope depth ($d_c$) was varied at 30 mm, 70 mm, and 110 mm, while the relative positions of the clip angles was kept at 20 mm below the top edge of the coped beam web (i.e., $p$=20 mm). As a result, the absolute positions ($p'$) of the angles were 50 mm, 90 mm, and 130 mm from the top flange, respectively. For the models of the connection position series, the cope depth ($d_c$) was kept at 30 mm, while the relative position of the clip angles ($p$) was varied at 20 mm, 60 mm, and 100 mm. The ratios of connected lengths of clip angles for all of these models was set at 2.4 ($a$=50 mm and $b$=120 mm). The analyses for these two series of models were carried out on two beam series, i.e. Beam356 ($t_w$=7.0 mm) and Beam457 ($t_w$=9.1mm), and the results are shown in Fig. 14. The figure shows that the capacity of both the Beam457 and Beam356 models decreased as cope depth increased. When the cope depth increased, the amount of web area in the cope region to carry the applied loading (shear and bending) was also reduced; hence, the connection capacity decreased.

The capacities of the models with tension fracture failure were slightly improved by lowering the clip angles connection (increasing $p$), as shown in Fig. 14. On the other hand, even though the vertical shear area path $b'$ *(which is equal to* $b + p$) increased when the connection was moved to a lower position, the capacities of the models with local web buckling failure did not improve. Lastly, the failure mode tended to change from the tension fracture mode to the local web buckling mode either when the coped depth was increased or when the connection position was lowered.

*5.4 Effect of the rotational stiffness of the clip angles*

In order to investigate the effect of the rotational stiffness of the double clip angles on the block shear capacity, a SPRING1 element was employ to simulate the bolted connections at the outstanding legs of the clip angles. As described in the section on the modeling of boundary conditions, at the outstanding legs of the double clip angles, vertical and out-of-plane displacements around the bolt holes were constrained ($U_2$ = 0, $U_3$ = 0). SPRING1 elements were used between the clip angles and the column flange, acting in the horizontal direction to simulate the effects of the deformation of the snug-tight bolts and washers. There were about 200 SPRING1 elements at the nodes around the holes. The spring tensile and compressive stiffness were varied between zero to infinity in order to simulate the effect of an ideal pin joint to an infinitely-restrained joint. Thus, the linear stiffness of each spring (force per relative displacement, $E_s$) was selected to be 0, 50, 200, 500, 1000, 2000, 10000 (units in N/mm), and infinity (i.e. $U_1$=0). The analyses were conducted on two series of Beam457 models ($a$ = 50 mm while $b$ = 120 mm and $a$ = 50 mm while $b$ = 200 mm with $d_c$ =30 mm and $c = a + 50$ mm for both series) as shown in Table 3, and the results are shown in Fig. 15. As can be seen from the figures, the capacity and failure modes of the models were sensitive to the spring stiffness. As the spring stiffness increased, the capacity improved significantly. By increasing $E_s$ from zero to infinity, a 42.2% or 24.5% increase in capacity was achieved when $b$ was 120 mm or 200 mm, respectively. The results also show that if the spring stiffness was less than 50 N/mm, the restraint could be treated as the pin joint ($E_s$=0 N/mm). However, if the spring stiffness was more than 10000 N/mm, the load deflection behavior was similar to that with infinite stiffness.

The pin joint was believed to generate insignificant end moments to the beam web, and therefore allowed flexible rotation of the connection to occur. Consequently, a

relatively large rotation of the connection induced tension fractures in the web material underneath the clip angles at a lower load. As the spring stiffness increased, local web buckling may dominate the ultimate failure mode. For example, for the models where *b* was 200 mm, if the spring stiffness was larger than 200 N/mm, local web buckling failure near the cope end would govern rather than block shear with tension fractures.

The calibrations of the finite element model by the test results verified that the bilinear springs could provide a reasonable prediction of strength for the test specimen while maintaining a close match with the actual load deflection curve. Although the results of the parametric study indicated that the rotational stiffness of the clip angles has a significant effect on the block shear strength of the coped beams, further experimental study is required to substantiate the research findings.

### *5.5 Stress distributions around the area of the clip angles*

The stress distributions around the web block near the welded clip angles were further investigated to reveal the relationship between the capacity and the connection geometry. The analyses were carried out based on Beam457, with a beam web thickness of 9.1 mm. A typical stress pattern is shown in Fig. 16 for the case of varying areas of tension. The results showed that at the ultimate failure stage, shear yielding developed in the shear area. The shear stresses varied from zero at the top edge of the beam web to an approximately trapezoidal distribution of shear stresses along the web shear area beside the edge of the clip angles. It was found that by increasing the shear area, the shear stresses became more uniform but the average stress decreased slightly. In addition, increasing the shear area could also lead to a decrease in the tensile stresses in the area of tension as shown in Fig. 16, since more of the total vertical reaction force was carried by shear. On the other hand, the ultimate tensile strength was reached in the tension area as shown in Fig. 16. The tensile stress was largest at the beam end and

decreased moderately along the length of the area of tension. Although the tensile stress distribution was generally nonlinear, for design practice the distribution of the tensile stresses can be treated approximately as a linear function. A further discussion on the proposed stress distribution around the web block will be presented below.

For the case with varying areas of tension, increasing the tension area would lead to a decrease the shear stresses in the shear area. However, the tensile stress distributions were almost identical (at both the elastic stage and the ultimate stage) when the area of tension was increased. Both the shear area and tension area did not have a significant effect on the tensile stress distribution in the tension area at the ultimate stage, where block shear failure with tension fractures occurred. A more detailed discussion of the stress distribution around the web block can be found in Zhong *et al.* [5].

## 6. Development of the modified design equation

### *6.1 General*

From the review of the current design standards, the existing design rules for block shear are mainly associated with bolted end connections. They do not provide sufficient design guidelines for block shear in coped beams, especially for welded end connections. The existing equations do not provide any insights on the variations in strength arising from changes in the geometry of the web block, and they often produce overestimations of connections with large areas of tension. Hence, a modified strength model, which can reflect the observed failure mode, needs to be developed in order to provide consistent predictions of the block shear of cope beams with welded end connections. The strength model for block shear should incorporate two terms: one reflecting the tensile resistance that develops along the horizontal plane, and the other

reflecting the shear resistance that develops along the vertical plane. The strength is the sum of the tensile resistance term and the shear resistance term. The following discussions present the development of the proposed design model.

*6.2 Proposed design model*

The design model is developed based on the test and the analytical results presented earlier. The basic form of the equation for the design model is similar to one of the existing AISC equations, that is:

$$P = F_u A_t + 0.6 F_y A_v \tag{3}$$

where:

$P$ is the ultimate connection capacity;

$F_u$ is the ultimate tensile strength;

$F_y$ is the yield strength;

$A_t$ is the tension area; and

$A_v$ is the shear area.

This equation assumes that the strength of the connection is the sum of the tensile strength in the tension area and the shear yield strength in the shear area around the web block. It should be noted that the proposed design model will only consider the effects of the connection geometry, namely, the aspect ratio of the clip angles (which includes the effect of both the tension and the shear areas). From both the experimental and the analytical results of this study, it was concluded that the aspect ratio of the clip angles has a significant effect on the block shear strength of coped beams.

Although, based on the parametric study, it appears that the influence of the rotation stiffness of the clip angles is also significant, further experimental work is required to verify the validity of the analytical results. Hence, the proposed design model in this study will not include the effect of rotational stiffness. Nevertheless, a further study to include both the effects of web block geometry and the rotational

stiffness of clip angles should be conducted in order to produce a comprehensive design model for the block shear of coped beams with a welded clip angles connection.

To account for the effects of the aspect ratio of the clip angles, correction factors ($R_t$ for the tension component and $R_v$ for the shear component) are applied to Eq. (3). The development of these factors is discussed below. It is observed from both the analytical and the experimental results that the tension area (in the horizontal plane) has a non-uniform tensile stress distribution. The stress is largest at the beam end and decreases along the tension area. As the length of the tension area increases, the decrease in the tensile stress is more obvious. Based on the stress distribution obtained from the results of the finite element analysis results, a trapezoidal tensile stress distribution can be assumed over this area. The schematic of the theoretical stress distribution of the proposed design model is presented in Fig. 17. It should be noted that the rate of decrease in the tensile stress (MPa/mm), $\varphi$, from the beam end along the horizontal plane is a function of the length of the tension area, $a$. That is, when $a$ is shorter, the tensile stress is more uniform. Meanwhile, at the stage when tension fractures occur, the true ultimate tensile strength, $(1+\varepsilon_u)\ F_u$, where $\varepsilon_u$ is the strain at the ultimate stress, has been achieved for the web material of the tension area near the beam end. Away from the beam end along the horizontal plane, the stresses decrease and can be smaller than $F_u$ when the tension area is large. Therefore, a factor, $k$, is used for the tensile stress away from the beam end. To simplify the model, the tension correction factor, $R_t$, is introduced such that the area of the trapezoidal stress block is the same as a rectangular stress block with a stress value of $R_tF_u$.

Based on the results of the finite element analysis presented in the previous section, the rate of decrease in the tensile stress, $\varphi$, versus the length of the tension area,

*a*, is shown in Fig. 18. The following linear approximation equation was obtained to relate $\varphi$ (MPa/mm) and *a* (mm):

$$\varphi = 0.0342a - 0.8231 \qquad 40 \le a \le 100 \text{ mm.} \qquad (4)$$

The corresponding stress factor, *k*, was obtained by the following equation:

$$k = (1 + \varepsilon_u) - \frac{\varphi a}{F_u} \qquad (5)$$

Therefore, the corresponding force contributed by the tensile stress is

$$\left[\frac{1 + \varepsilon_u + k}{2}\right] F_u A_t \qquad (6)$$

By substituting Eq. (5) into (6) and assuming $\varepsilon_u$ to be 0.2 in this case, the following expression for $R_t$ is obtained:

$$R_t = \left(1.2 - \frac{\varphi a}{2F_u}\right) \qquad (7)$$

Therefore, the tensile component of the block shear strength can be expressed as $R_t F_u A_t$.

The shear stress is assumed to distribute uniformly along the vertical edge of the clip angle. Although the shear stress is difficult to evaluate, it is known from the test and analytical results that the shear stresses along the vertical plane were less than the shear fracture strength. Hence, the shear yield stress (approximately equal to $0.6F_y$) along with a shear stress correction factor, $R_v$, is used to estimate the effective shear stress,

expressed as $R_v \cdot 0.6F_y$, in the shear area. An examination of the shear stress distribution from the analytical results revealed that the magnitude of the effective shear stress was mostly influenced by the connection geometry. As shown in Fig. 19, the average shear stress along the shear area decreases as *a* increases. On the other hand, the influence of the length of the shear area, *b*, does not seem to be significant. Therefore, based on the results of the finite element analysis, the shear stress correction factor $R_v$ is expressed in terms of the connection geometry, *a*. Fig. 20 shows the plot of $R_v$ versus *a*, and a linear approximation was obtained to relate $R_v$ and *a* (mm).

$$\mathrm{R_v} = 1.5528 - 0.0078a \qquad 40 \le \mathrm{a} \le 100 \text{ mm} \tag{8}$$

Moreover, recall that a triangular shear stress distribution is assumed to vary from zero to $0.6R_vF_y$ for the shear area between the top edge of the beam web and the angle (Fig. 17). As a result, the total force contributed by the shear area can be expressed by the following equation:

$$\mathrm{R_v}(0.6\mathrm{F_y})\mathrm{A_v} + 0.5\mathrm{R_v}(0.6\mathrm{F_y})\mathrm{p}t_w \tag{9}$$

Since there are no bolt holes for the welded clip angles connection; hence, the gross area of the relevant plane is used. To compute accurately for the connected length, the fillet weld size (*s*) is considered in the area terms of the equation. Based on the above discussion, the proposed design equation for predicting the block shear strength of a welded clip angles connection is given as follows:

$$\mathrm{P_r} = \mathrm{R_t F_u}(a + \mathrm{s})\mathrm{t_w} + 0.6\mathrm{R_v F_y}(b + s + 0.5\mathrm{p})t_w \tag{10}$$

where $R_t$ is the tension correction factor (Eq. (7)), $R_v$ is the shear correction factor (Eq. (8)) $a$ is the length of the tension area, $b$ is the length of the shear area, $t_w$ is the thickness of the beam web, $s$ is the size of the fillet weld, and p is the distance between the angle and the top edge of the beam web.

## 7. Evaluation of the proposed modified design equation

The block shear design equations prescribed by the current standards of CSA-S16-01 [7] and AISC LRFD [8] are shown as follows:

CSA-S16-01 (2001):

$$P_r = \phi(0.5F_u A_{nt} + 0.6F_y A_{gv}) \tag{11}$$

$$P_r = \phi(0.5F_u A_{nt} + 0.6F_u A_{nv}) \tag{12}$$

AISC LRFD (1999):

If $F_u A_{nt} \geq 0.6F_u A_{nv}$: $\quad P_r = \phi(F_u A_{nt} + 0.6F_y A_{gv}) \leq \phi(F_u A_{nt} + 0.6F_u A_{nv})$ (13)

If $F_u A_{nt} < 0.6F_u A_{nv}$: $\quad P_r = \phi(F_y A_{gt} + 0.6F_u A_{nv}) \leq \phi(F_u A_{nt} + 0.6F_u A_{nv})$ (14)

where $P_r$ is the ultimate connection capacity (the lesser value of the above equations), $\phi$ is the resistance factor, $F_u$ is the tensile strength, $F_y$ is the yield strength, $A_{nt}$ is the net tension area, $A_{gv}$ is the gross shear area, $A_{nv}$ is the net shear area, and $A_{gt}$ is the gross tension area.

The major difference between the CSA and AISC predictions of block shear strength is that a triangular stress block with a maximum stress of $F_u$ is assumed for the tension area in the CSA equations; therefore, the contribution of the tension area is

reduced by one-half (Kulak and Grondin [9]). Comparing the test data in the literature, the AISC prediction seems to give a better prediction than the CSA prediction. However, the predictions by CSA are generally more conservative than those by AISC.

The comparison of the capacities predicted by the proposed design equation (Eq. (10)) with results of both the finite element analysis and the test for the block shear failure mode is presented in Fig. 21. The professional factor (defined as the test/analytical results-to-predicted ratios) varied from 0.89 to 1.12, with a standard variation of 0.063. The predictions by the CSA-S16-01 [7] and the AISC LRFD [8] standards, the two representative standards in North America, are also included in Fig. 21. It can be seen from the figure that the CSA-S16-01 [7] gave very conservative predictions. Meanwhile, the results predicted by both AISC and the proposed design equations were close to the results of the finite element analysis. Moreover, it was found that the variation in the professional factor for AISC LRFD [8] predictions was 0.81 to 1.15 with a standard variation of 0.093, which were larger than those of the proposed design equation. This indicates that the proposed design equation provides a better prediction for block shear failure than the other two existing standards.

Although the proposed design equation gives better prediction of the block shear capacity of coped beams with welded connection details, some of the predicted capacities are still non-conservative. In order to provide a conservative design and to account for other factors that are not included in the proposed design equation, it is recommended that the ultimate strain be reduced from 0.2 to 0.05.. With this modification, Eq. (7) is changed to the following:

$$R_t = \left(1.05 - \frac{\varphi a}{2F_u}\right) \qquad (15)$$

With the above modification, the variation in the professional factor of both the results of the finite element analysis and the test for the block shear failure mode is 0.99 to 1.21, with a standard variation of 0.058. The corresponding plot of the results is shown in Fig. 22.

As mentioned above and also in Yam *et al.* [1], local web buckling was also one of failure modes for the test specimens. Although some of the test specimens failed due to the local buckling of the web, these specimens exhibited significant deformation of the block shear type prior to reaching their final failure mode. Hence, it is believed that the proposed design equation may be able to give an indication of the capacities of the specimens. The comparisons of the capacities predicted by the proposed design equation (Eq. 10 - $\varepsilon_u$ = 0.2, 0.05) with the test results for the specimens with the web buckling failure mode are presented in Fig. 23. The predictions by the CSA-S16-01 [7] and the AISC LRFD [8] standards are also included in the figure. It can be seen from the figure that the CSA-S16-01 [7] gave conservative predictions. On the other hand, the results predicted by AISC gave non-conservative predictions. The predictions by using Eq. 10 (with $\varepsilon_u$ = 0.05) are close to the test results. However, since the failure mode of those specimens was local web buckling, a design equation that reflects the actual failure mode should be developed for better predictions.

## 8. Design example

For the purpose of illustration, consider the design of a coped beam with a welded clip angles connection with respect to block shear, as shown in Fig. 24. This section and the cope details are identical to the test specimen C2. The beam web ($t_w$) equals 9.2 mm, the length of the tension area ($a$) equals 50 mm, the length of the shear

area ($b$) equals 120 mm, the connection position ($p$) equals 20 mm, and the fillet weld size ($s$) equals 12 mm. The yield strength $F_y$ is 371.6 MPa, and the ultimate tensile strength $F_u$ is 487.7 MPa.

The effective tension area, $A_t$, is:

$$A_t = (a+s)t_w = (50+12)\times 9.2 = 570.4 \text{ mm}^2.$$

The effective shear area, $A_v^{'}$, is:

$$A_v^{'} = (b+s+0.5p)t_w = (120+12+0.5\times 20)\times 9.2 = 1306.4 \text{ mm}^2.$$

The tensile correction factor $R_t$ is given by Eq. 7 as:

$$R_t = 1.05 - \frac{0.0342a^2}{2F_u} + \frac{0.8231a}{2F_u} = 1.05 - \frac{0.0342\times 50^2}{2\times 487.7} + \frac{0.8231\times 50}{2\times 487.7} = 1.01$$

The shear stress correction factor $R_v$ is:

$$R_v = 1.5528 - 0.0078a = 1.5528 - 0.0078\times 50 = 1.16$$

Thus, the resistance to block shear can be obtained by Eq. 10:

$$P_r = R_t F_u A_t + 0.6 R_v F_y A_v^{'}$$

$$= 1.01\times 487.7\times 570.4 + 0.6\times 1.16\times 371.6\times 1306.4$$

$$= \mathbf{618.8\ kN}$$

The predictions according to CSA-S16-01 [7] and AISC LRFD [8] are 399.3 kN and 511.5 kN, respectively (without considering the safety factor, $\phi$). The corresponding test result of the ultimate reaction for this connection is 630.0 kN. Both the CSA and AISC code gave conservative predictions even though the safety factor was not considered in the prediction. The prediction by using the proposed design equation is within 2% of the test result.

## 9. Conclusions

A finite element analysis of the block shear capacity of coped beams with welded clip angle connections was presented in this paper. The finite element model was calibrated by a testing program conducted by Yam *et al.* [1]. The calibrated finite element model was then used to conduct a parametric study. The parameters included: (1) the aspect ratio of the clip angle, (2) the shear and tension areas, (3) the cope length, cope depth, and connection position, and (4) the rotational stiffness of the clip angles.

Based on both the test and the analytical results, the following conclusions were drawn:

1. The block shear and local web buckling failure modes may occur in cope beams with welded end connections.
2. The geometry of the web block will affect the strength and the failure mode of the connection. Connection capacity increases as the aspect ratio of the clip angle (the area that connected to the beam web) increases, but the rate of increase will become small if the aspect ratio is large.
3. The influence of the shear area on the connection capacity is more pronounced than the tension area. Local web buckling rather than tension fractures will occur if the shear area is large.
4. A large area of tension will increase loading eccentricity and hence generate more bending moments to the edge of the beam web region near the clip angles.
5. The beam section depth, cope depth, and connection position did not greatly affect the connection capacity. However, if the coped depth was increased or the

connection position was lower, local web buckling of the coped beam tended to occur.

6. Increasing the tension area will lead to a decrease in the shear stresses in the shear area.

7. Based on the limited test and analytical results, a design equation for evaluating the block shear strength of coped beams with welded clip angles was proposed. However, care should be taken when using this equation for significantly different welded connections and coping details.

8. Further experimental and numerical studies are required to incorporate in the proposed design equation the effect of the rotational stiffness of clip angles, which has a significant effect on the block shear strength of the coped beams.

9. Although the proposed design equation was developed for predicting block shear, it does provide a reasonable estimation of the capacities of the specimens that failed due to local web buckling.

## 10. Acknowledgment

The authors would like to extend their gratitude to the Research Committee of the University of Macau for providing financial support for this project.

## 11. References

[1] Yam, CHM, Zhong, YCJ, Lam, CCA, and Iu, VP. “An investigation of the block shear strength of coped beams with a welded clip angles connection – Part I: Experimental study,” *Journal of Constructional Steel Research (companion paper)*.

[2] *ABAQUS/Standard User's Manual Version 6.3*, Hibbitt, Karlsson & Sorensen, Inc., 2002.

[3] Khoo, HA, Cheng, JJR, and Hrudey, TM, Determine steel properties for large strain from a standard tension Test, *Proceedings of the 2nd Material Specialty Conference of the Canadian Society for Civil Engineering*, Montreal, Quebec, Canada, 2002.

[4] Cheng, JJR, and Kulak, GL, Gusset plate connection to round HSS tension members, *Engineering Journal*, Fourth Quarter, pp.133-139, 2000.

[5] Zhong, YCJ. Investigation of block shear of coped beams with welded clip angles connection. MSc thesis, University of Macau, Macau, 2004.

[6] Steel Construction Institute, *Steelwork design guide to BS5950: Part 1:1990. Volume. 1: Section properties, member capacities*, 4th edition, 1997.

[7] Canadian Standards Association (CSA). *Limit states design of steel structures*, *Standard CSA-S16-01*, Toronto, Ont., 2001.

[8] American Institute of Steel Construction (AISC). *Load and resistance factor design specification for structural steel buildings*, Chicago, IL, USA, 1999.

[9] Kulak, GL, and Grondin, GY, AISC LRFD rules for block shear in bolted connections – a review, *Engineering Journal,* AISC, 38(4): 199–203. See also "Errata and Addendum," *Engineering Journal*, AISC, 39(2), 2001

[10] Franchuk, CR, Driver, RG, and Grondin, GY, Block shear failure of coped steel beams, *Proceedings of 4th Structural Specialty Conference of the Canadian Society for Civil Engineering*, Montreal, Quebec, Canada, 2002

[11] Franchuk, CR, Driver, RG, and Grondin, GY, Experimental investigation of block shear failure in coped steel beams, *Canadian Journal of Civil Engineering*, Vol. 30, No. 5 , pp. 871-881, 2003.

**Table 1 Summary of the parameters for the material models**

| **Beam A, B** | | **Beam C, D** | | **Beam E** | | **Clip Angle** | | **General** | |
|---|---|---|---|---|---|---|---|---|---|
| E = 191 GPa | | E = 203 GPa | | E = 204 GPa | | E = 203 GPa | | E = 205 GPa | |
| $\sigma_{True}$ (MPa) | | $\sigma_{True}$ (MPa) | | $\sigma_{True}$ (MPa) | | $\sigma_{True}$ (MPa) | | $\sigma_{True}$ (MPa) | |
| Yield | Ultimate | Yield | Ultimate | Yield | Ultimate | Yield | Ultimate | Yield | Ultimate |
| 319 | 683 | 372 | 750 | 305 | 685 | 306 | 760 | 321 | 706 |

**Table 2 Comparison of the results of the finite element analysis and the test**

| Specimen | Test Ultimate Reaction (kN) | FEA | | Test Failure Mode | FEA Prediction |
|---|---|---|---|---|---|
| | | Predicted Capacity (kN) | Test / Predicted | | |
| A1 | 395.2 | 409.8 | 0.96 | Buckling | Buckling |
| A2 | 437.4 | 437.5 | 1.00 | Buckling | Buckling |
| B1 | 394.0 | 419.4 | 0.94 | Buckling | Buckling |
| B2 | 390.3 | 396.7 | 0.98 | Buckling | Buckling |
| D1 | 623.0 | 629.3 | 0.99 | Buckling | Fracture |
| E2 | 581.0 | 567.1 | 1.02 | Buckling | Buckling |
| **Average** | | | 0.98 | | |
| C2 | 630.0 | 623.3 | 1.01 | Fracture | Fracture |
| E1 | 601.2 | 563.9 | 1.07 | Fracture | Fracture |
| **Average** | | | 1.04 | | |
| C1 | 690.1 | 780.1 | > 0.89 | Exceeded* | Fracture |
| D2 | 684.5 | 703.6 | > 0.97 | Exceeded* | Fracture |

**Note:** * Failure did not take place at the maximum applied load of the test setup.

**Table 3 Summary of the variables of the parametric study**

| Parameter | Beam356 series D=360, B=170, T=15.7 | | | Connection details |
|---|---|---|---|---|
| Web thickness, $t_w$ | 5.8 | 7.0 | 9.1 | |
| Aspect ratio, b'/a | 1.4, 2.3, 3.6 | 1.4, 2.3, 3.6 | 1.4, 2.3, 3.6 | See note 2 |
| Cope depth, $d_c$ | | 30, 70, 110 | | a = 50, b = 120 |
| Connection position, p | | 20, 60, 100 | | a = 50, b = 120 |

| Parameter | Beam457 series D=460, B=190, T=14.5 | | | Connection details |
|---|---|---|---|---|
| Web thickness, $t_w$ | 7.6 | 9.1 | 11.4 | |
| Aspect ratio, b'/a | 1.4, 2.3, 3.6, 4.8 | 1.4, 2.3, 3.6, 4.8 | 1.4, 2.3, 3.6, 4.8 | See note 2 |
| Shear area, b | | 120, 160, 200<br>120, 140, 160 | | a = 50<br>a = 70 |
| Tension area, a | | 50, 70, 90<br>50, 70, 100 | | b = 120<br>b = 160 |
| Cope length, c | 0, 50, 100, 150, 200 | 0, 50, 100, 150, 200 | 0, 50, 100, 150, 200 | a = 50<br>b = 120 |
| Cope depth, dc | | 30, 70, 110 | | a = 50<br>b = 120 |
| Connection position, p | | 20, 60, 100 | | a = 50<br>b = 120 |
| Spring stiffness, $E_s$ | | 0, 50, ..., inf<br>0, 50, …, inf | | a = 50, b = 120<br>a = 50, b = 200 |

Note:

1. All dimensions are in mm.
2. The aspect ratios of 1.4, 2.3, 3.6, and 4.8 represent the ratio of connected lengths of clip angles, i.e. b/a = 100/90, 140/70, 160/50, and 170/40, respectively.
3. The cope length in each model was kept at a constant distance of 50 mm extending from the end of the angles (i.e., c=a+50 mm), unless stated otherwise.
4. The cope depth in each model was kept at a constant distance of 30 mm from the top flange of the beam except for the cope depth series of models.
5. The connection position for the clip angles in each model was kept at a constant vertical distance of 20 mm from the top edge of the beam web, except for the connection position series of models.
6. The spring stiffness of the SPRING1 element was employed to produce the rotational stiffness of clip angles. The linear stiffness was selected to be 0, 50, 200, 500, 1000, 2000, 10000, and infinity. The unit is in N/mm.

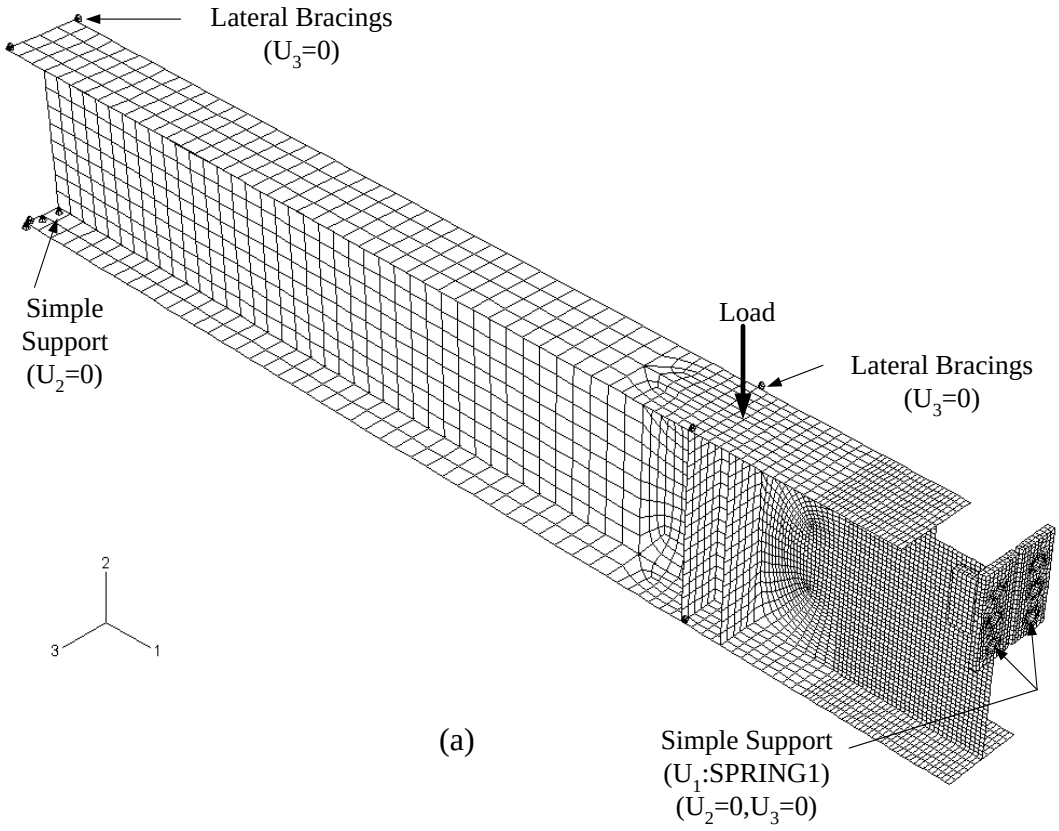


(a)

Simple Support
($U_1$:SPRING1)
($U_2$=0,$U_3$=0)

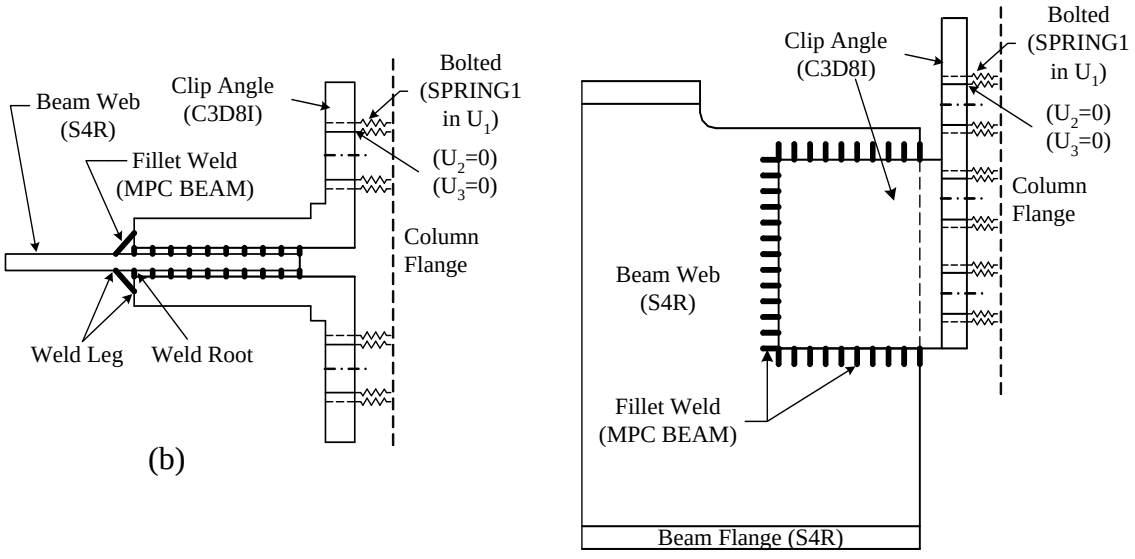


(b)

(c)

**Figure 1 Typical finite element model and boundary conditions**

(a)

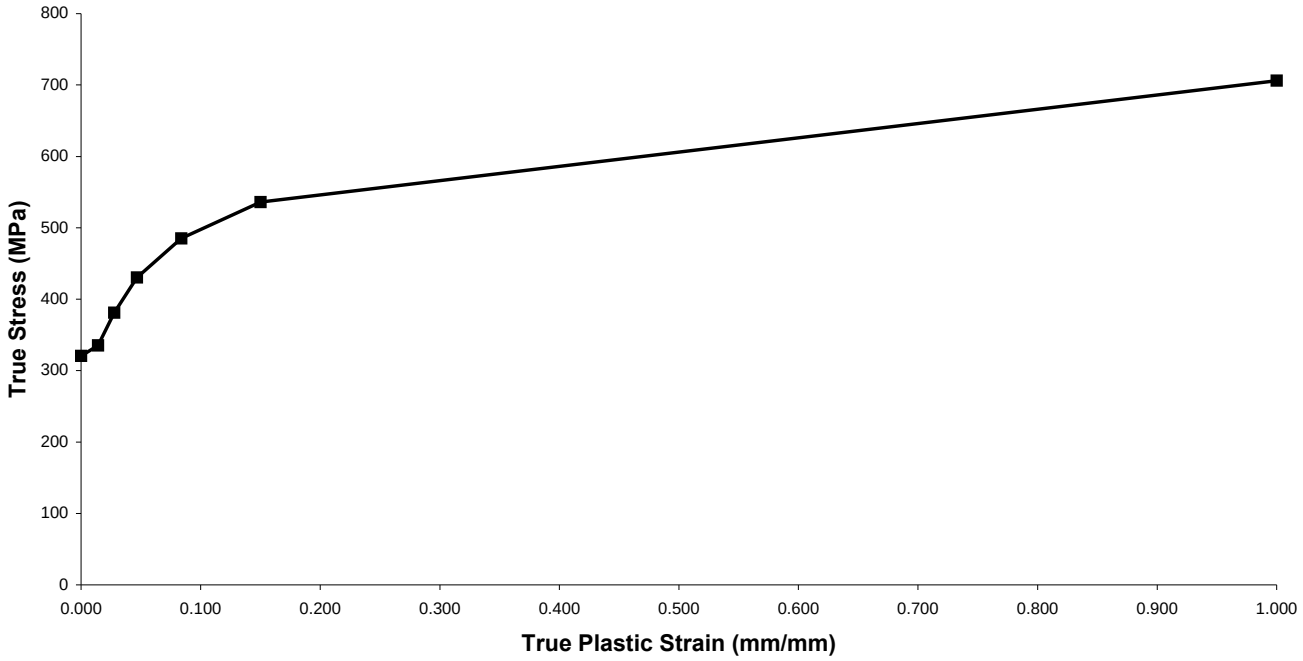


**Figure 2 Typical true stress vs. the true strain curve**

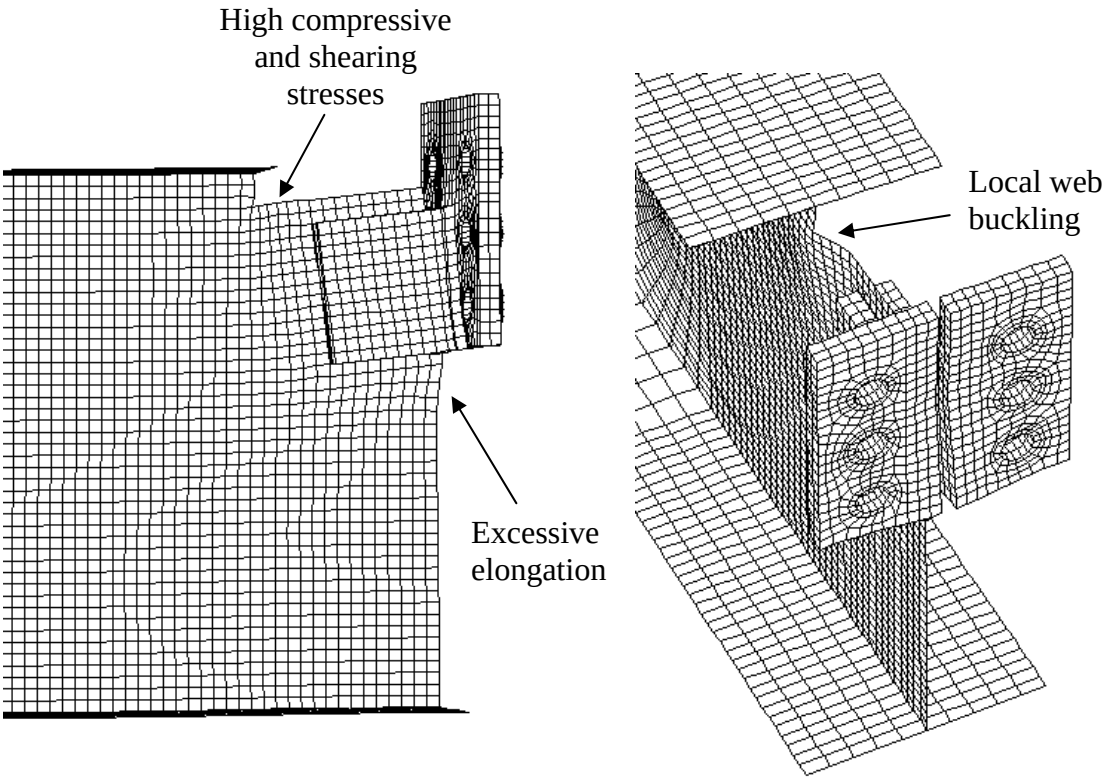


**Figure 3 Typical deformed shapes of the connection**

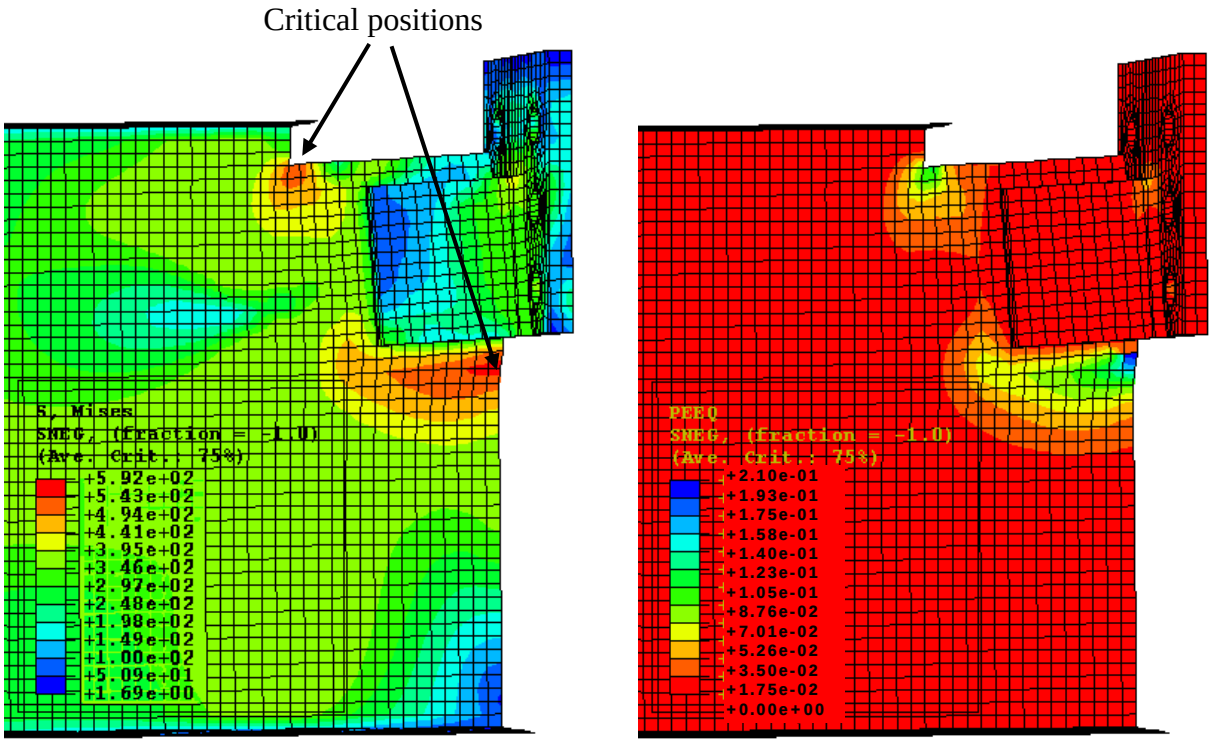


**Stress contours** **Equivalent plastic strain contours**

**Figure 4 Stress contours and equivalent plastic strain contours of model D1**

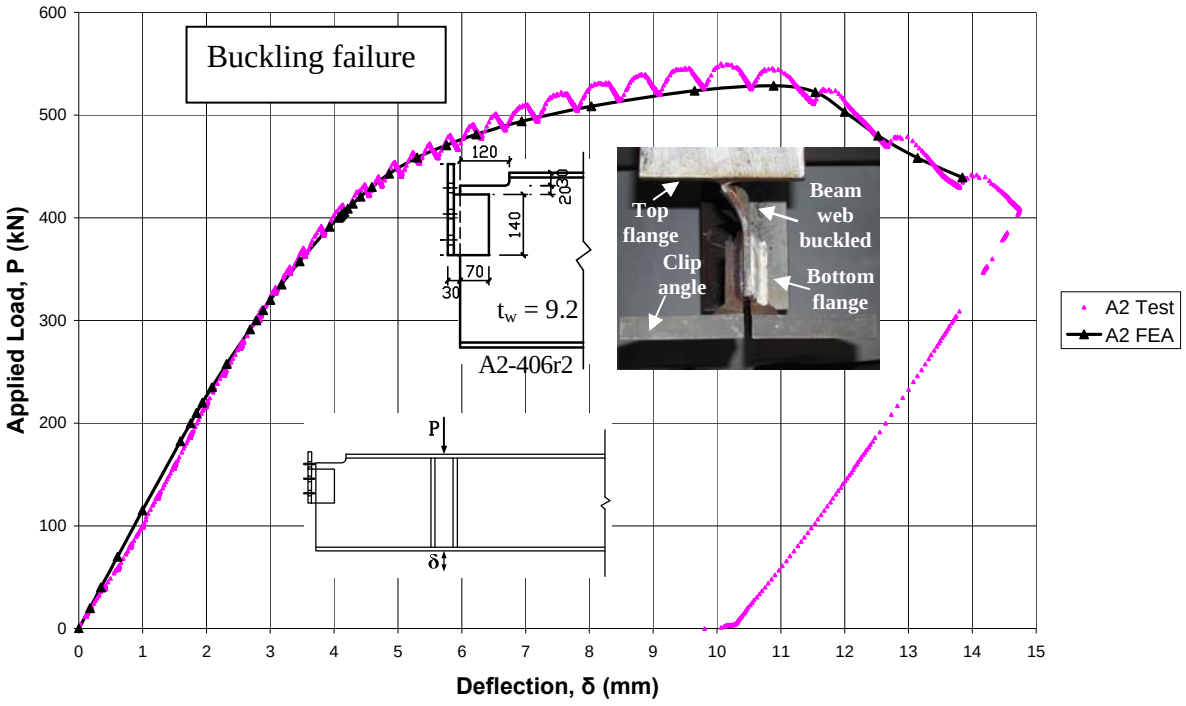


(a) specimen A2-406r2

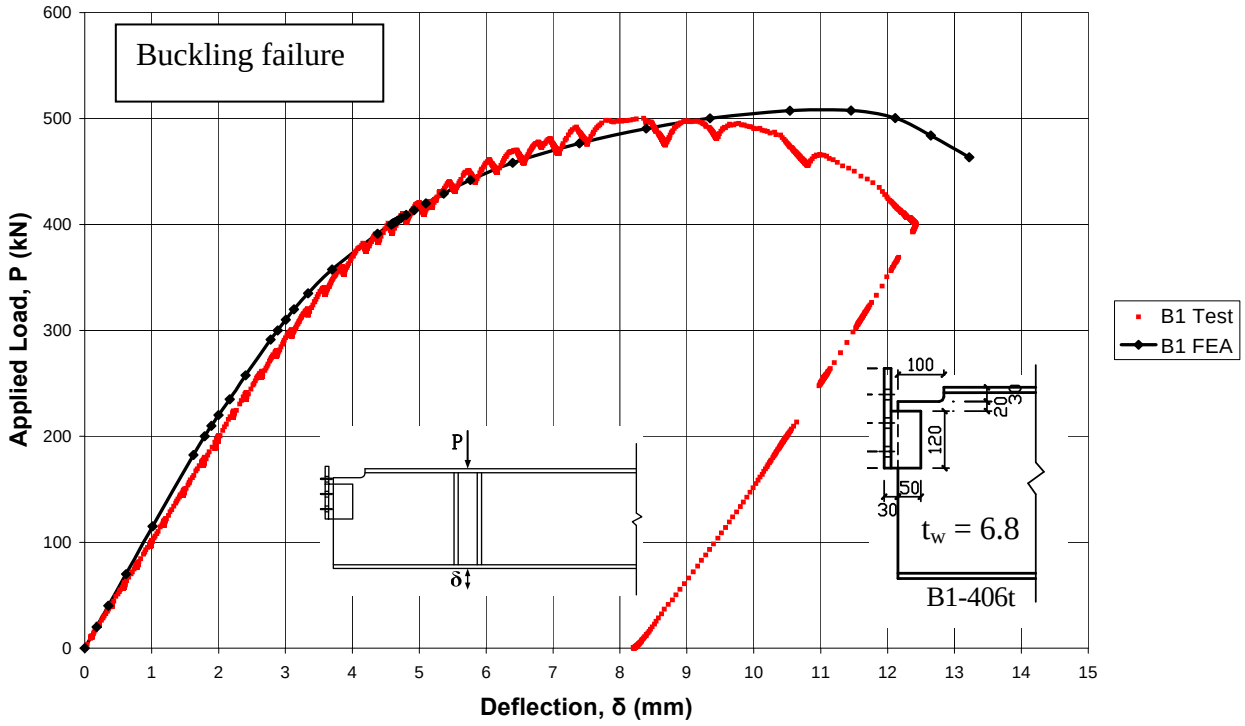


(b) specimen B1-406t

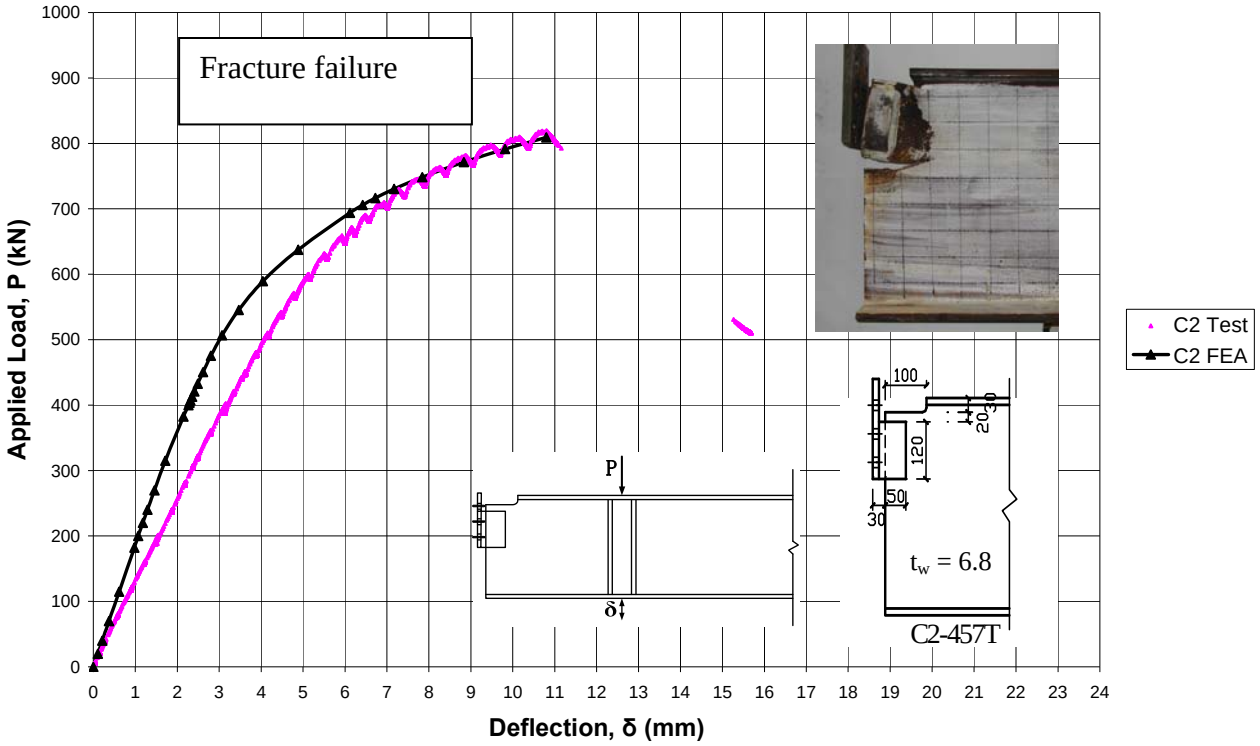


(c) specimen C2-457T

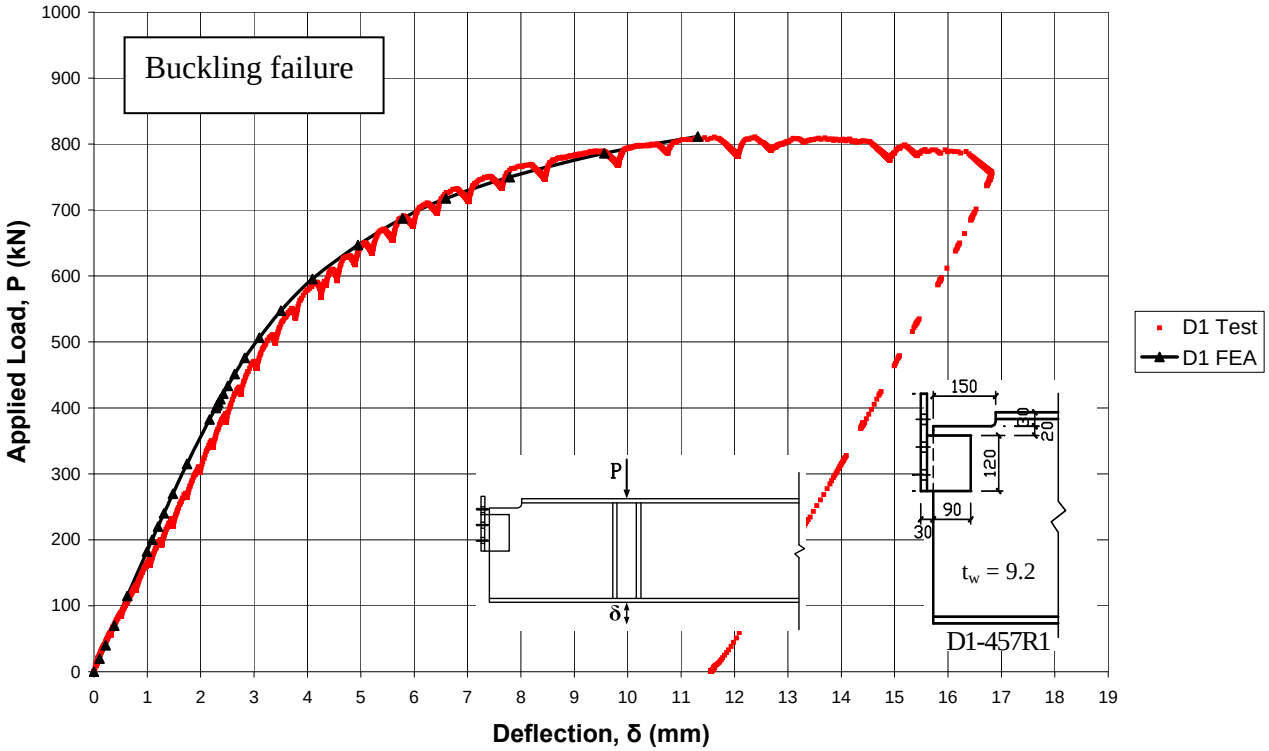


(d) specimen D1-457R1

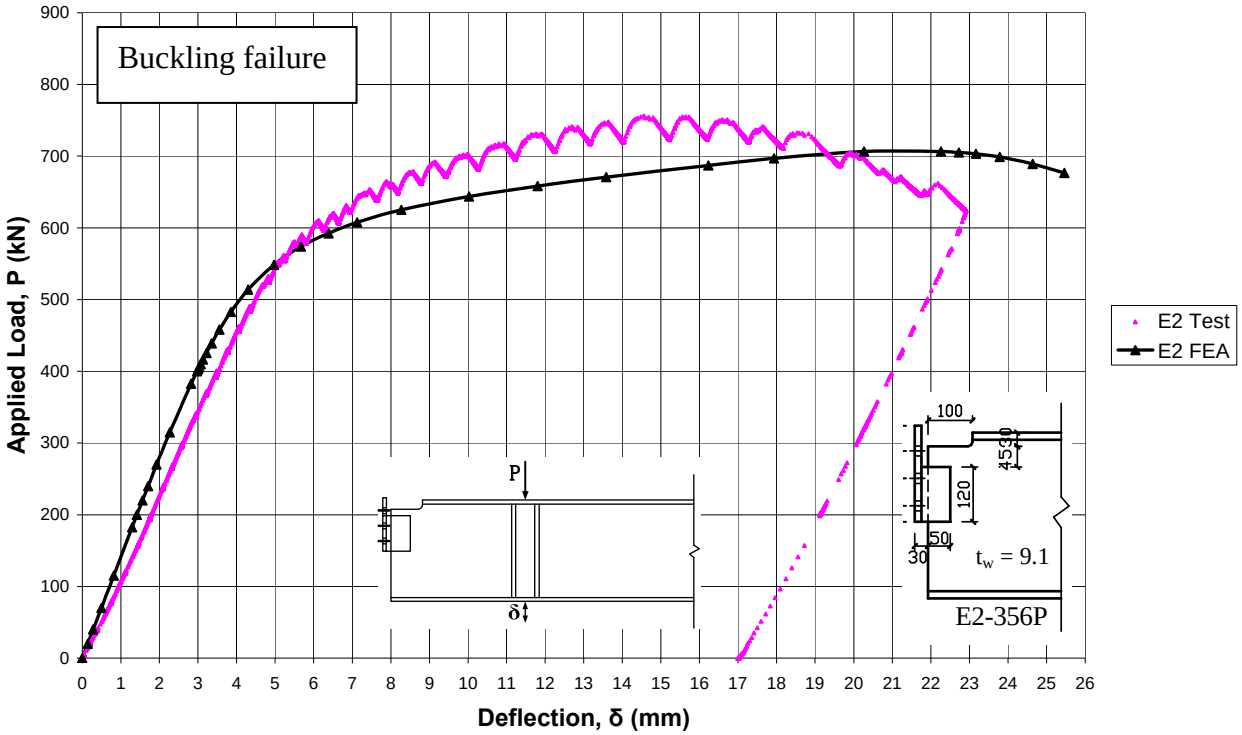


(e) specimen E2-356P

**Figure 5 Load vs. deflection curves for specimens A2-406r2, B1-406t C2-457T, D1-457R1 and E2-356P**

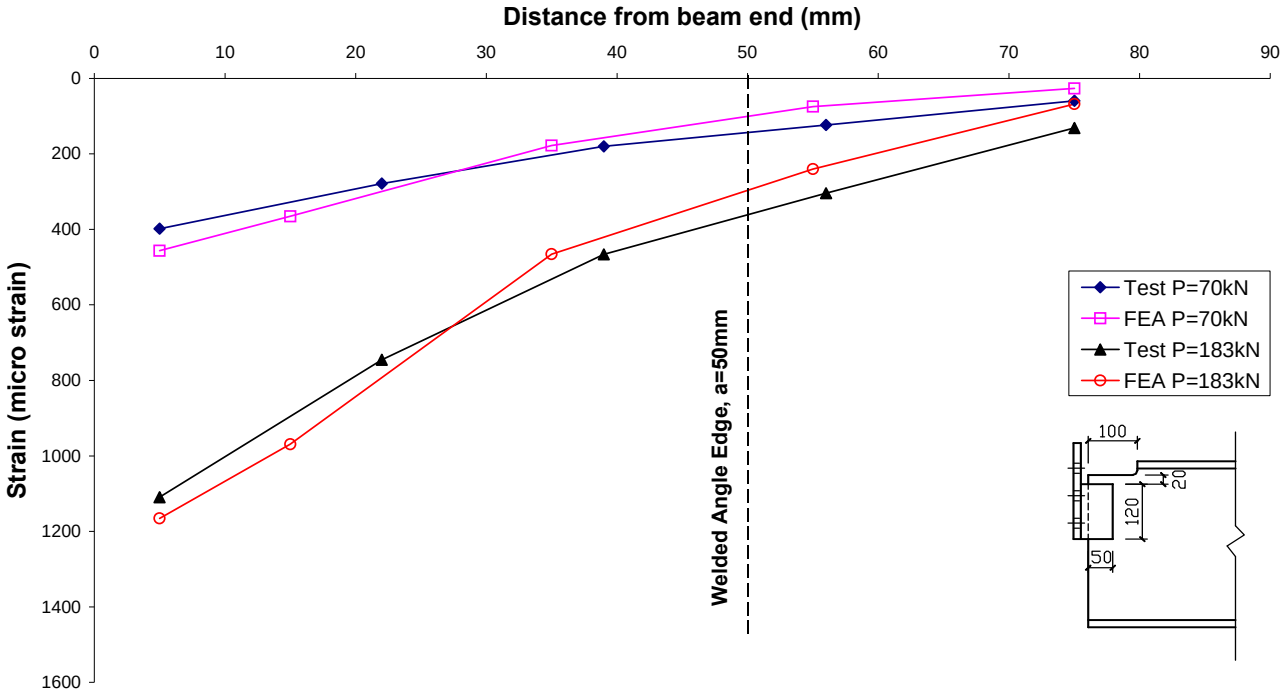


**Figure 6 Comparison of the tensile strain distribution along the tension area for specimen E1**

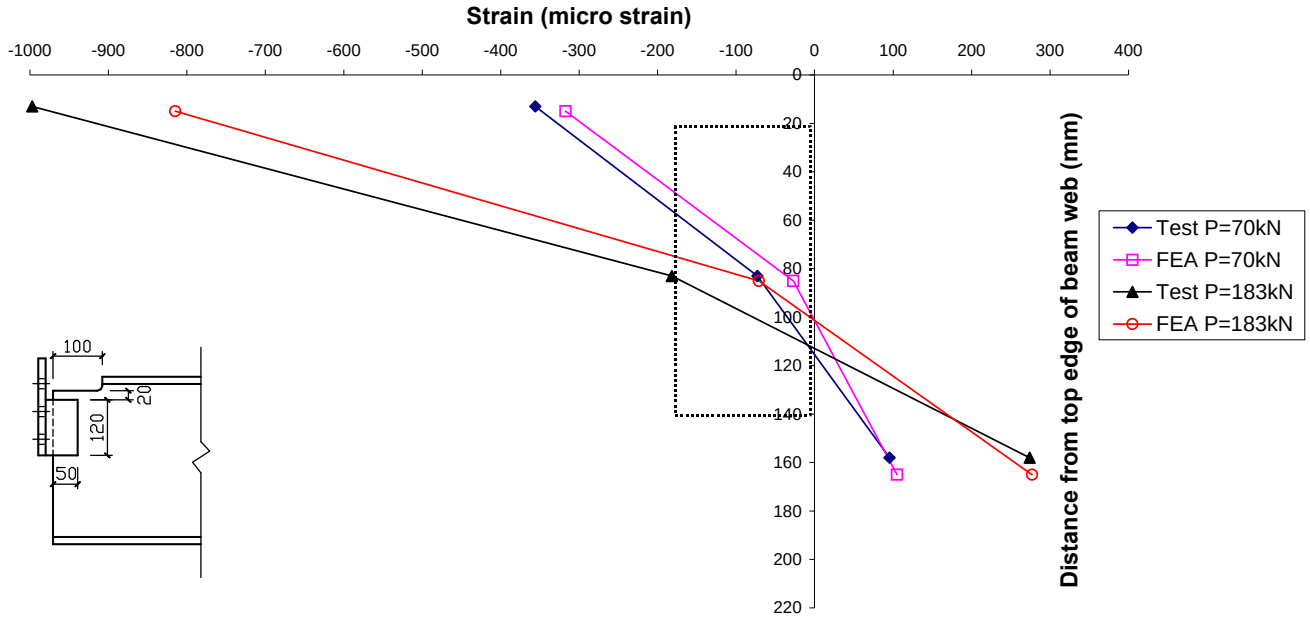


**Figure 7 Comparison of the flexural strain distribution along the shear area for specimen E1**

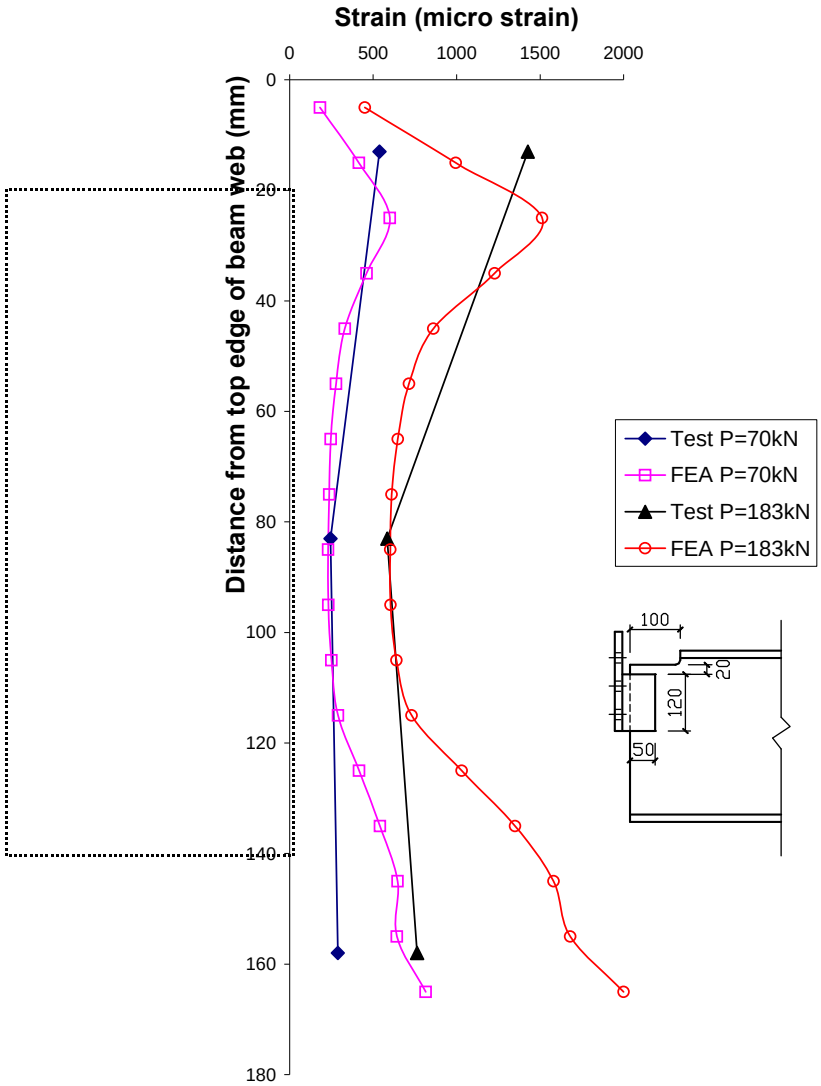


**Figure 8 Comparison of the shear strain distribution along the shear area for specimen E1**

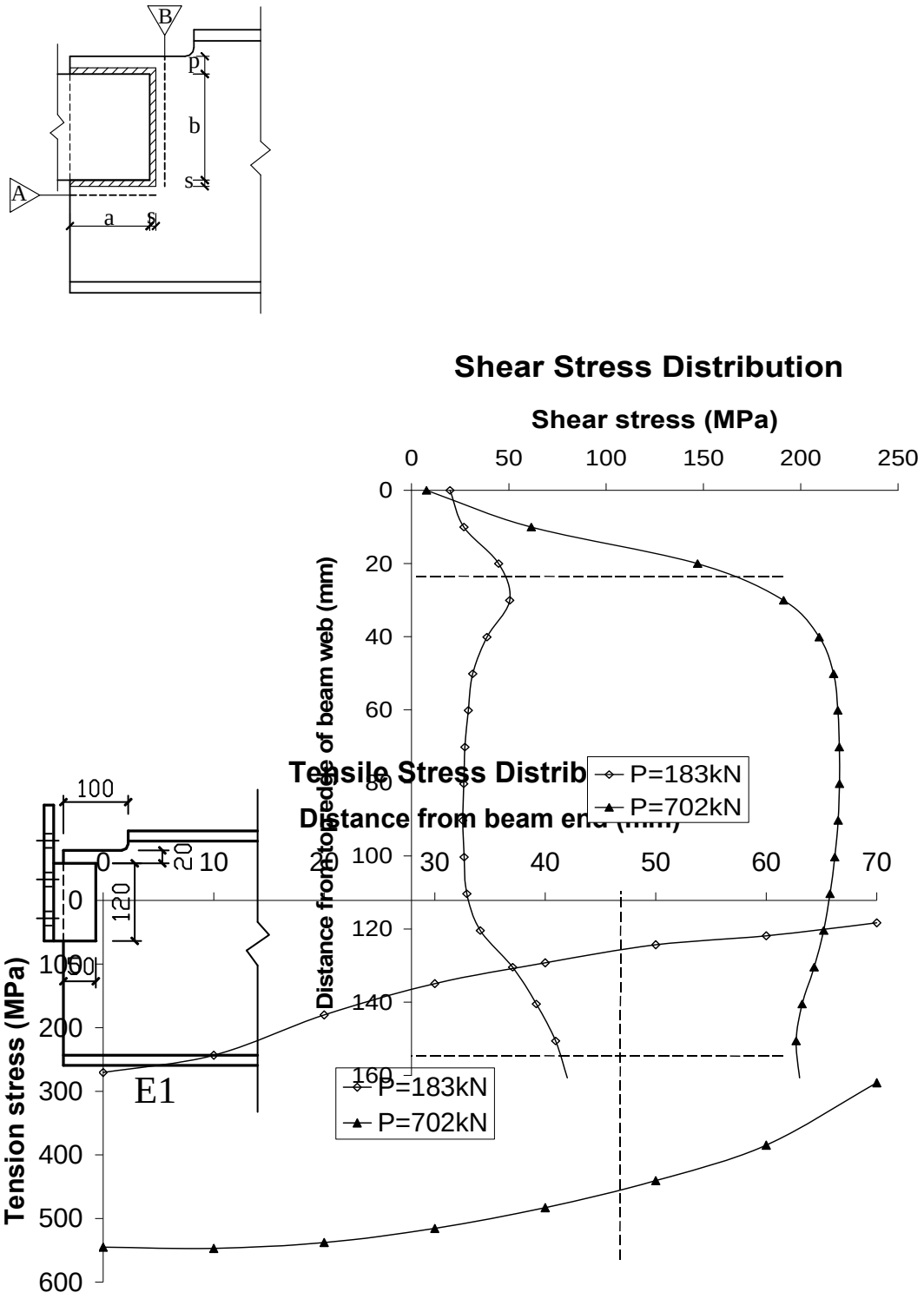


**Figure 9 Stress distribution around the clip angle of specimen E1-356T**

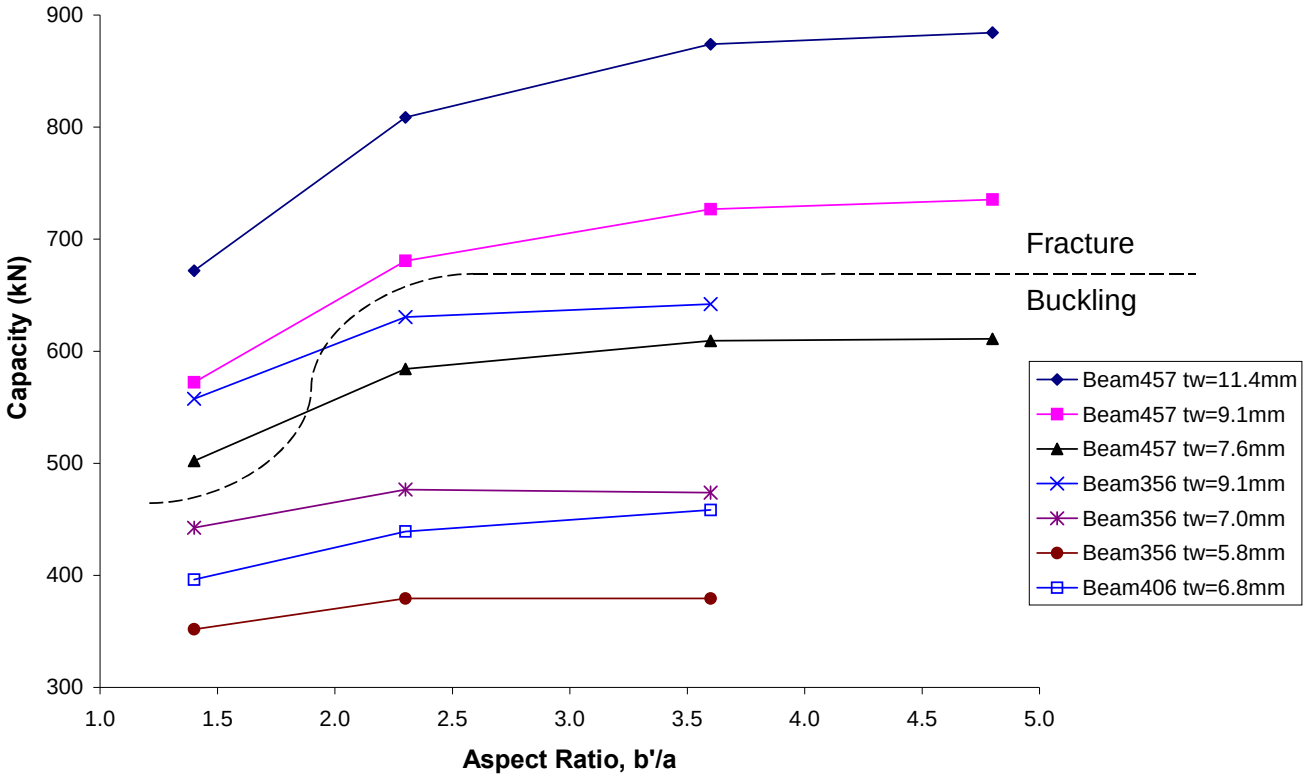


**Figure 10 Effects of aspect ratio**

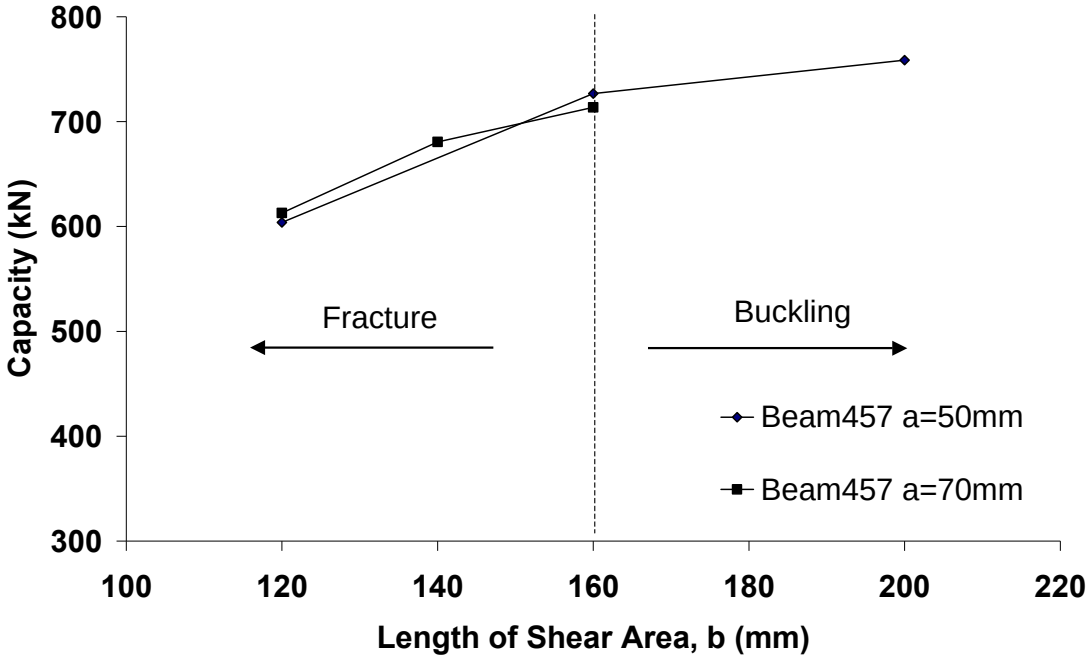


**Figure 11 Effects of shear area**

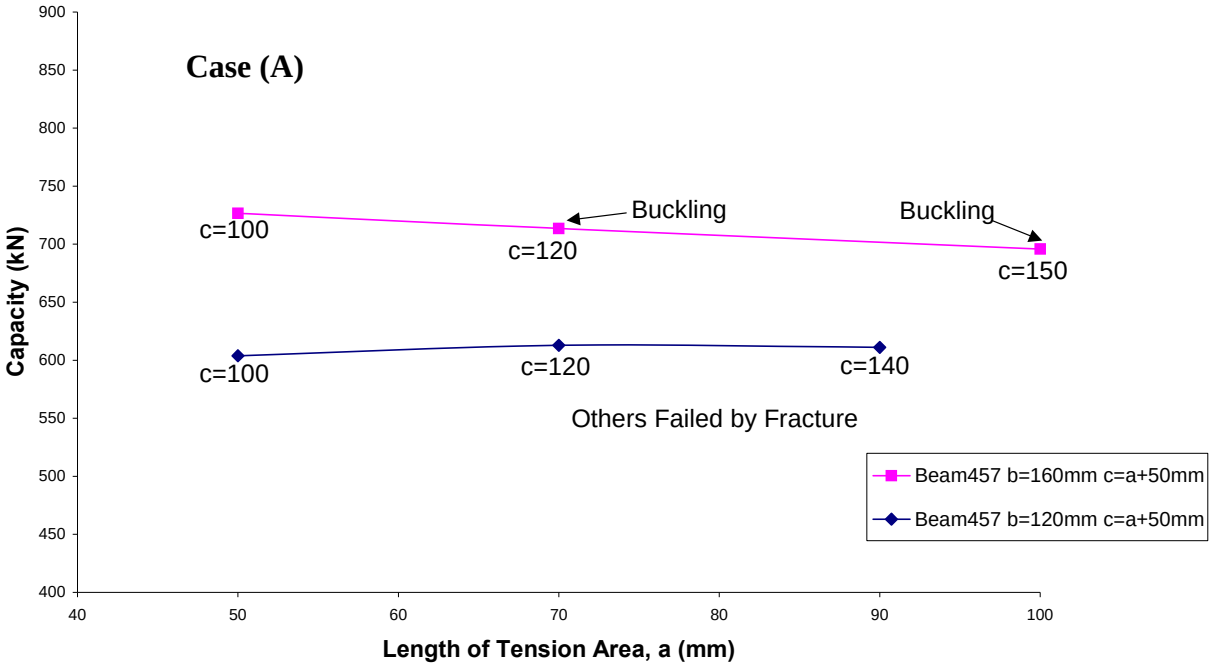


**(a)**

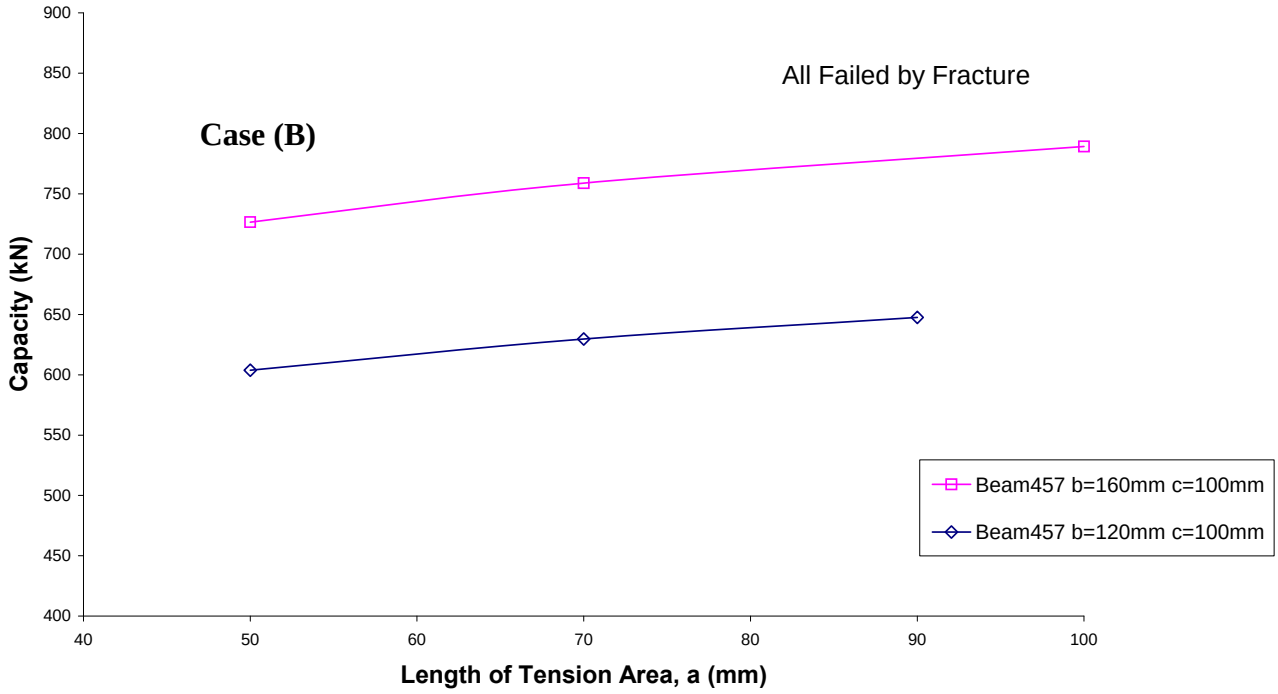


**(b)**

**Figure 12 Effects of tension area**

a = 50 mm and
b = 120 mm

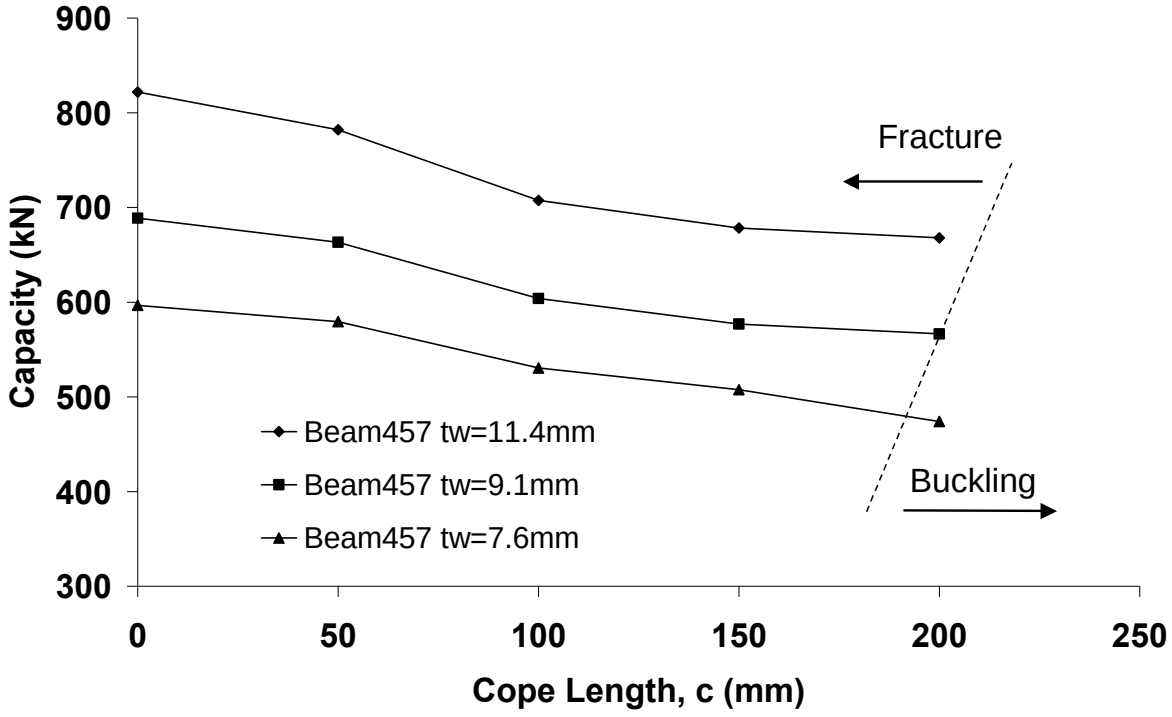


**Figure 13 Effects of cope length**

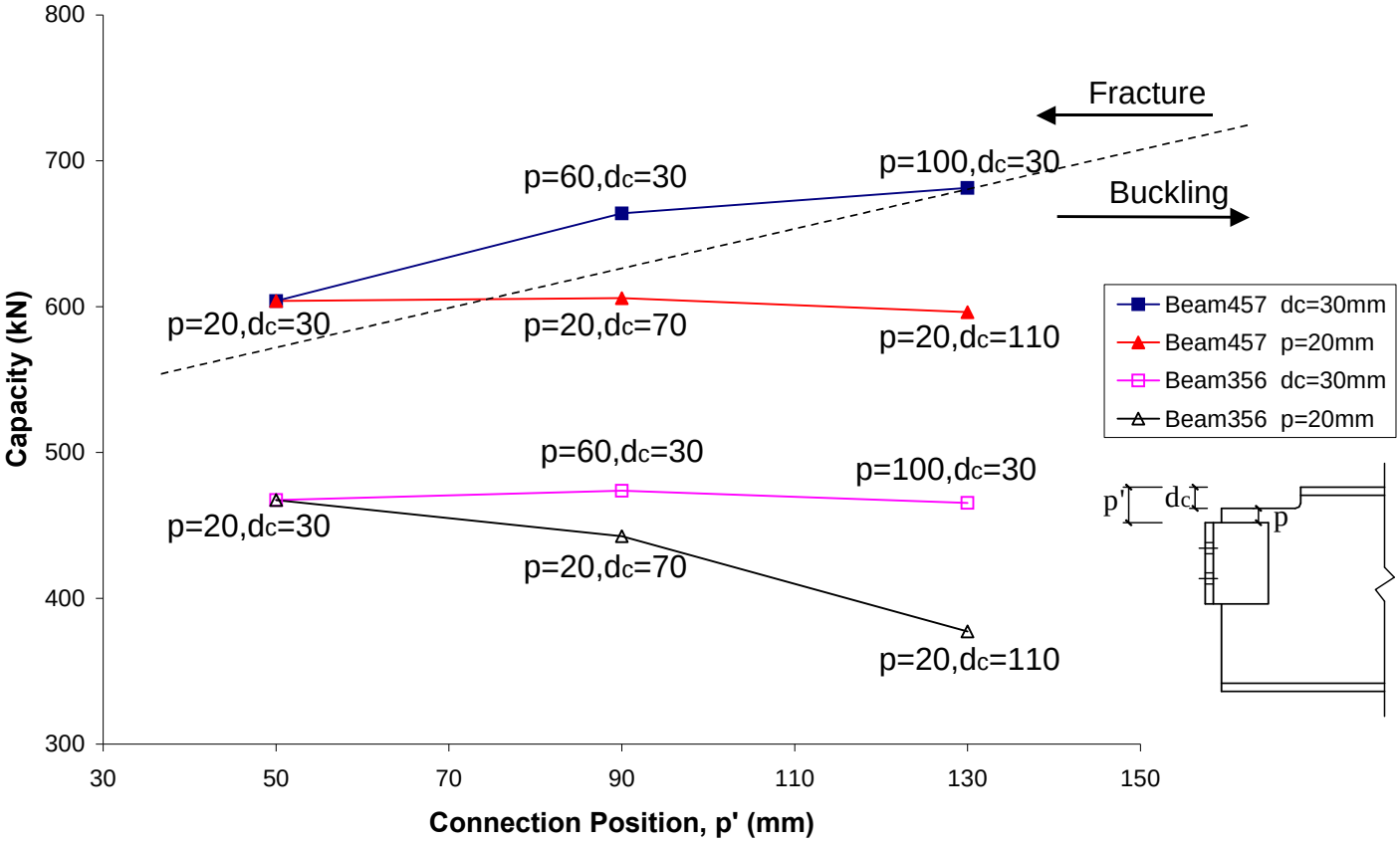


**Figure 14 Effects of cope depth and connection position**

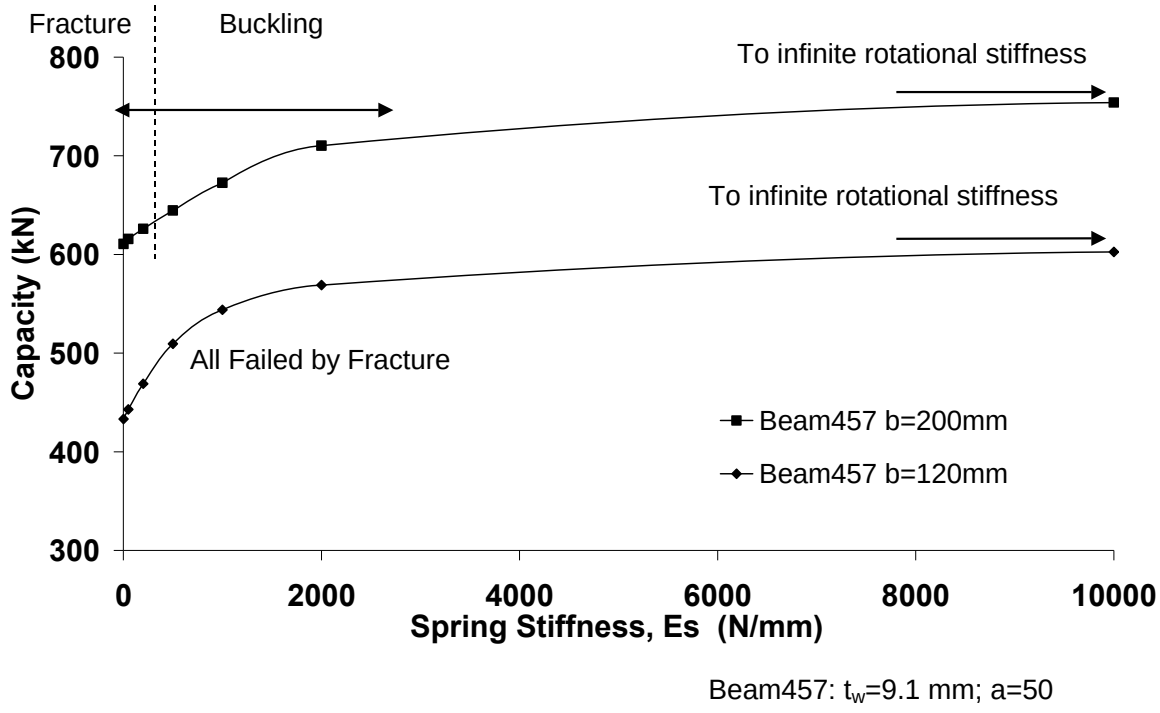


**Figure 15 Effect of the different rotational stiffness of the clip angles**

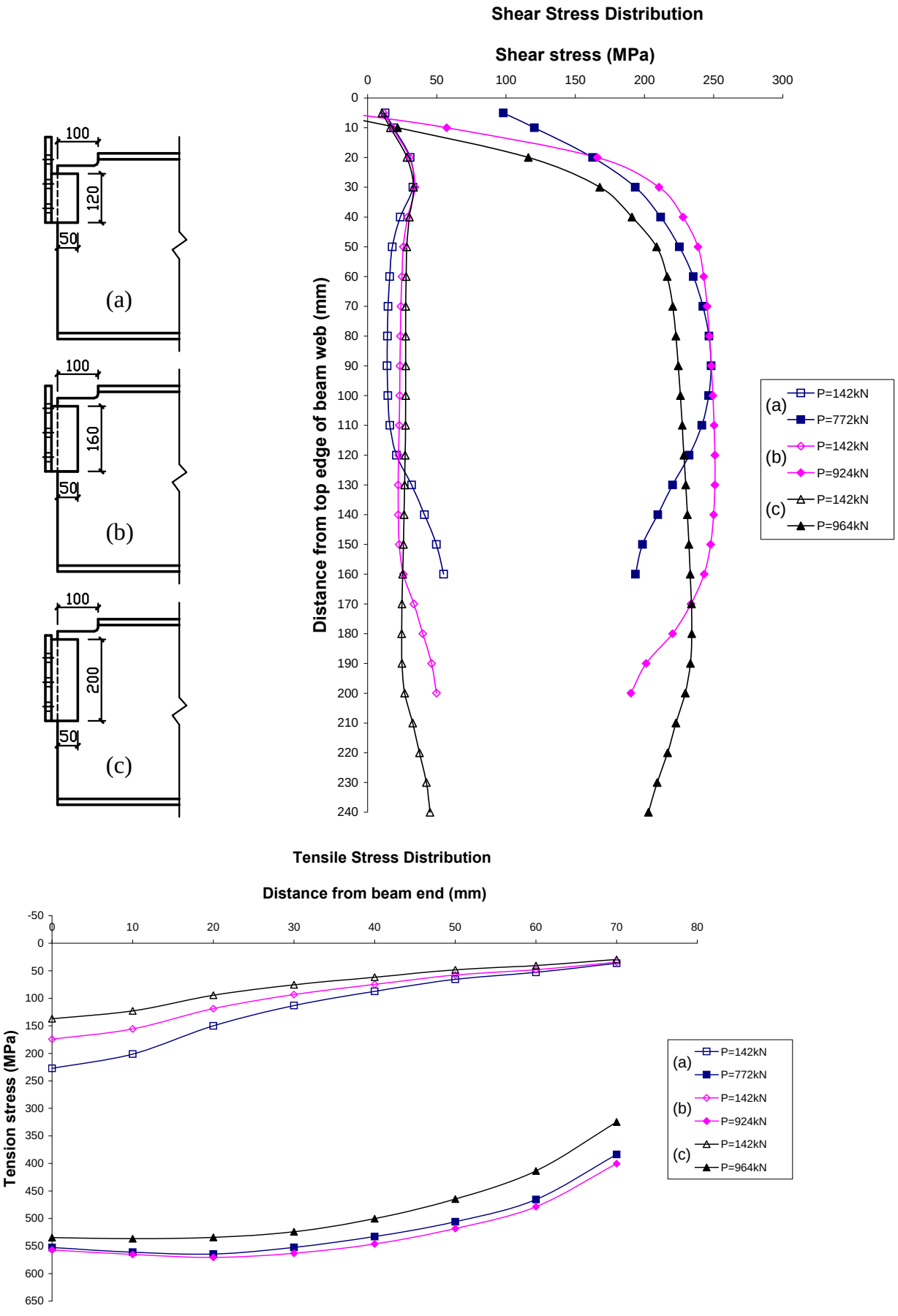


**Figure 16 Typical stress pattern for shear area series**

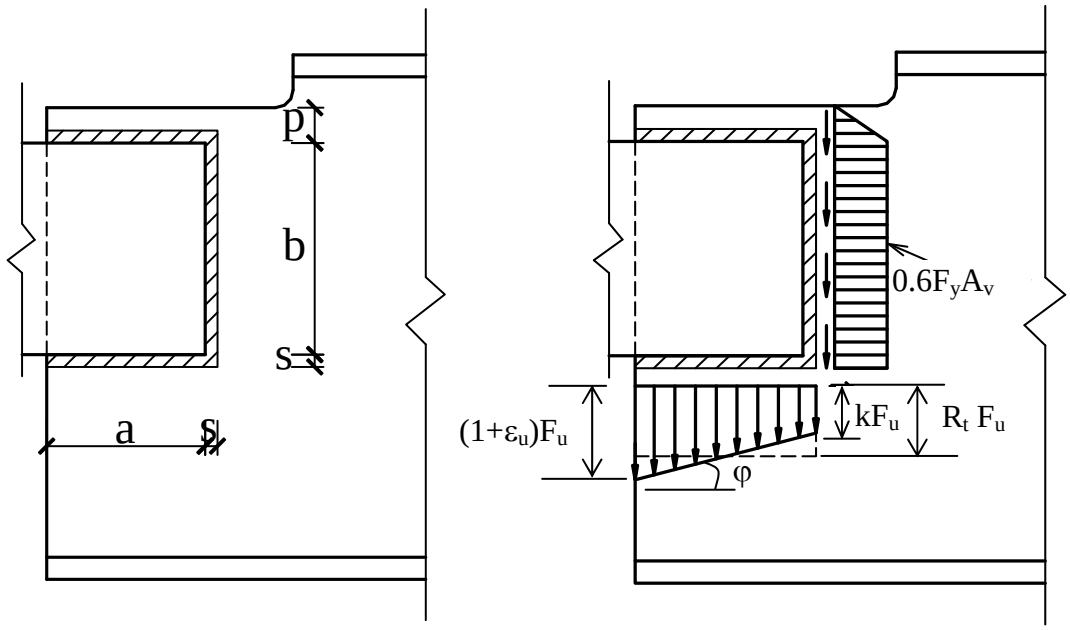


**Figure 17 Schematic of the theoretical stress distribution of the proposed strength model**

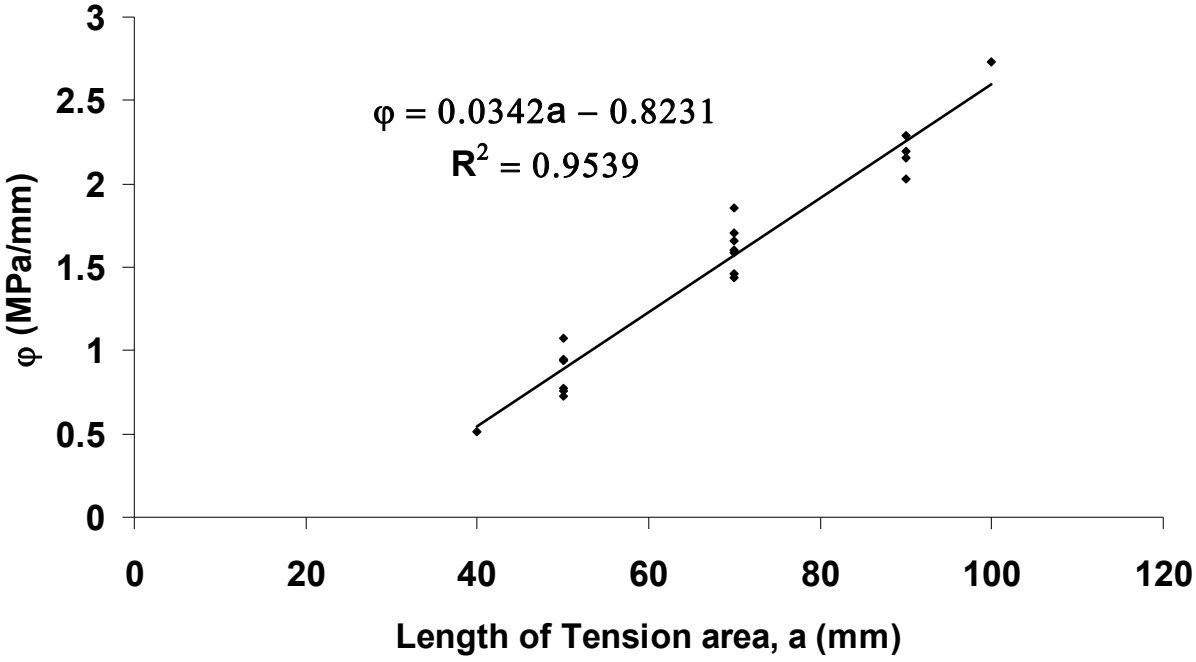


**Figure 18 Linear regression for φ vs. a**

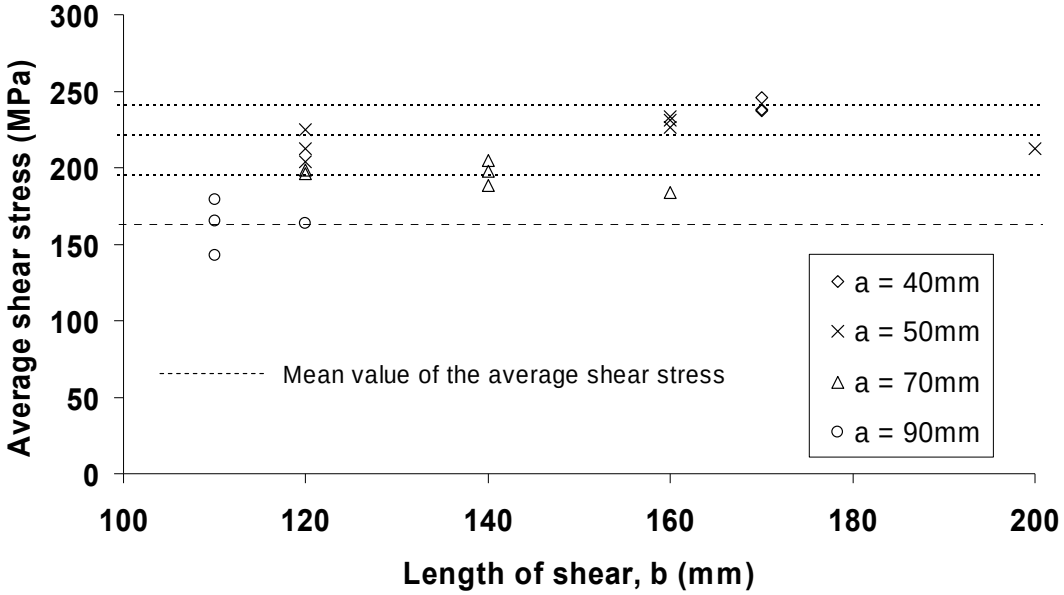


**Figure 19 Average shear stress vs. the length of the shear area**

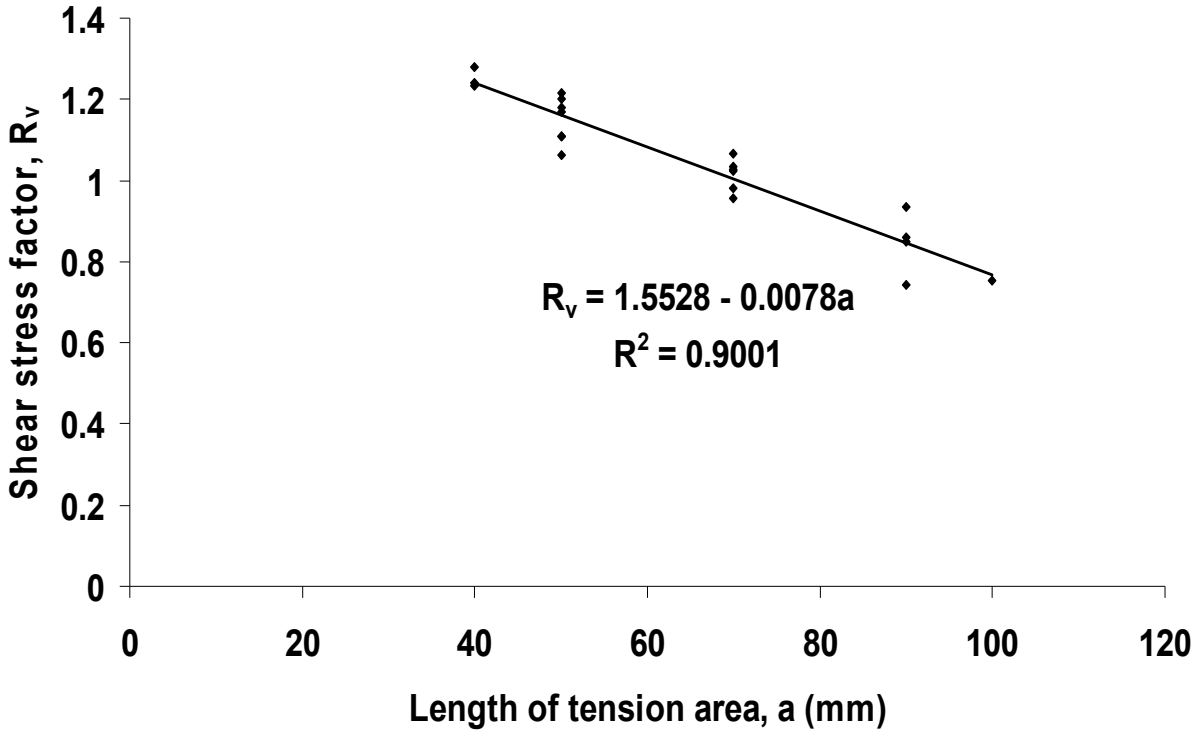


**Figure 20 Regression line for $R_v$ vs. a**

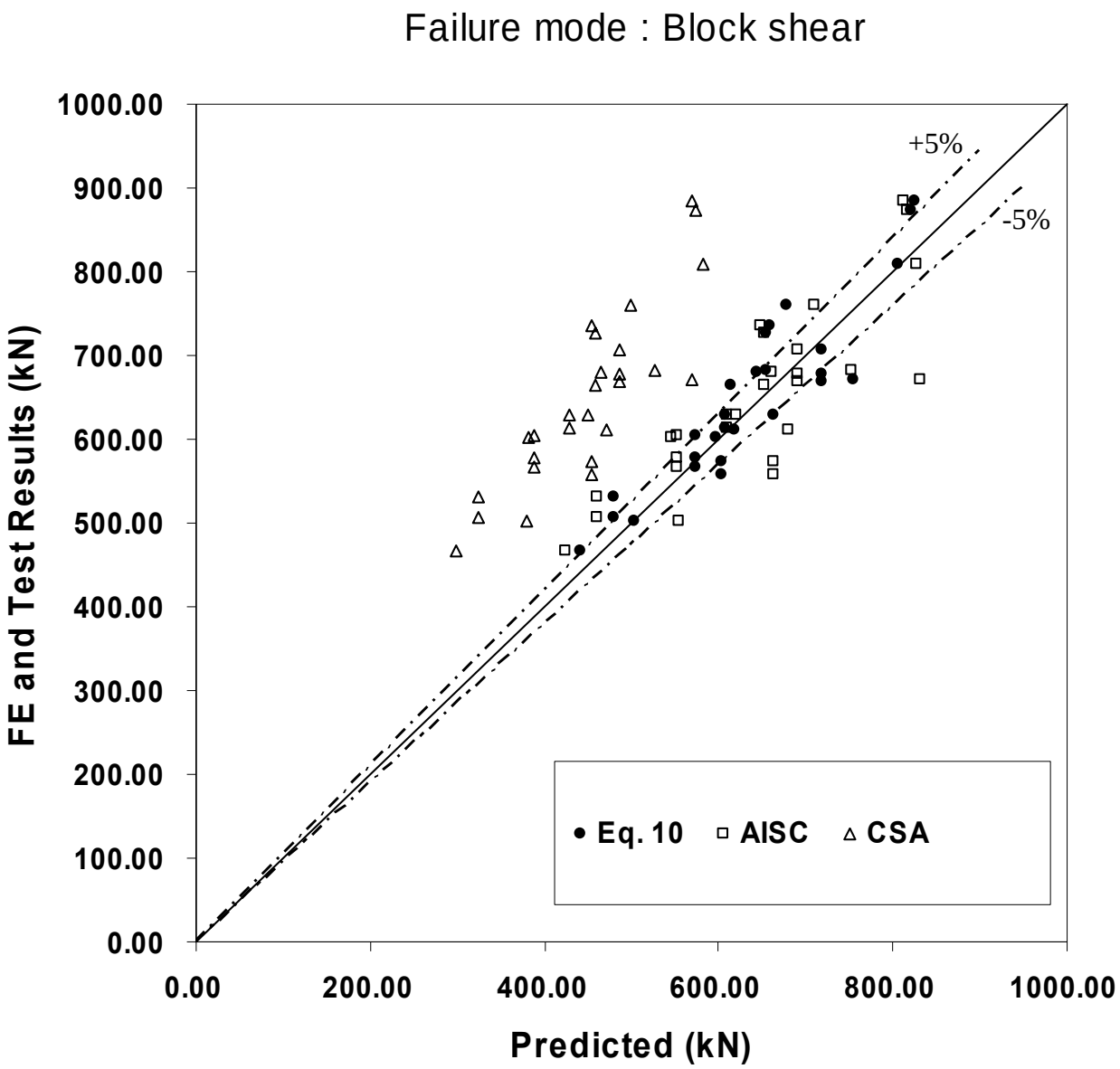


**Figure 21 Comparison of the predictions of the proposed design equation (Eq. 10 – $\varepsilon_u$ = 0.2) with FE and the Test results (Block shear failure mode)**

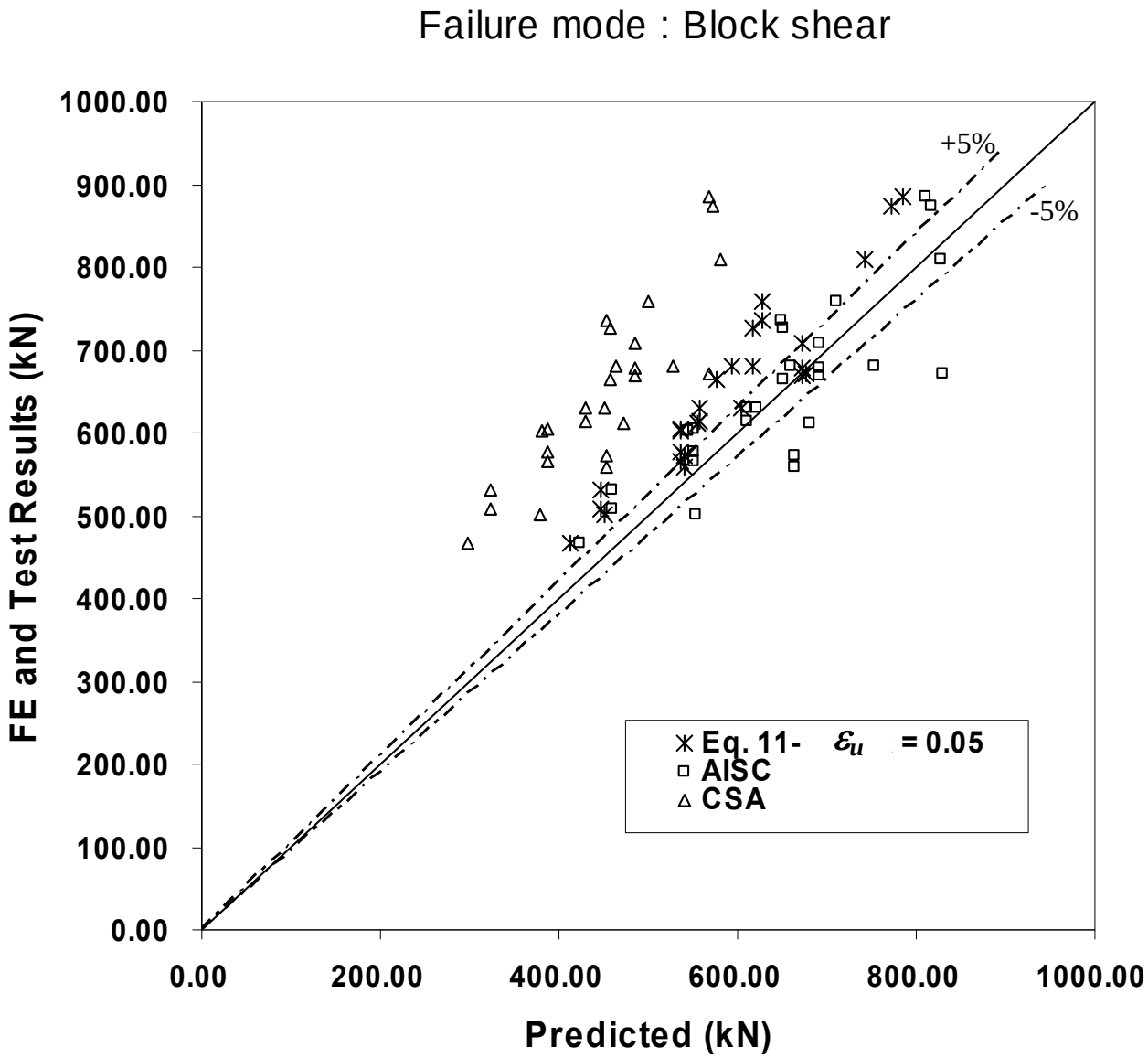


**Figure 22 Comparison of the predictions of the proposed design equation (Eq. 10 – $\varepsilon_u$ = 0.05) with the FE and Test results (Block shear failure mode)**

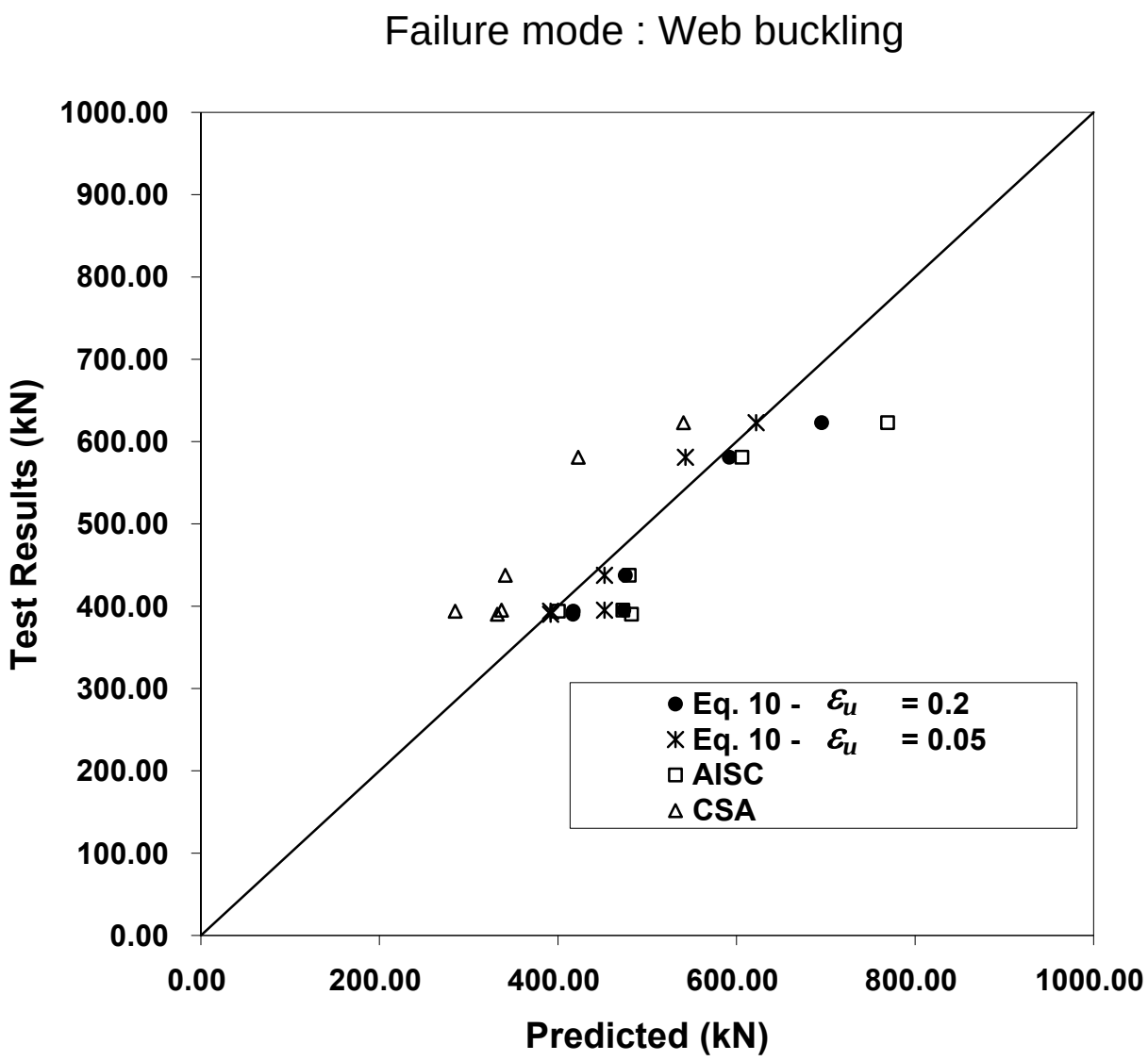


**Figure 23 Comparison of the predictions of the proposed design equations (Eq. 10) with the test results (Web buckling failure mode)**

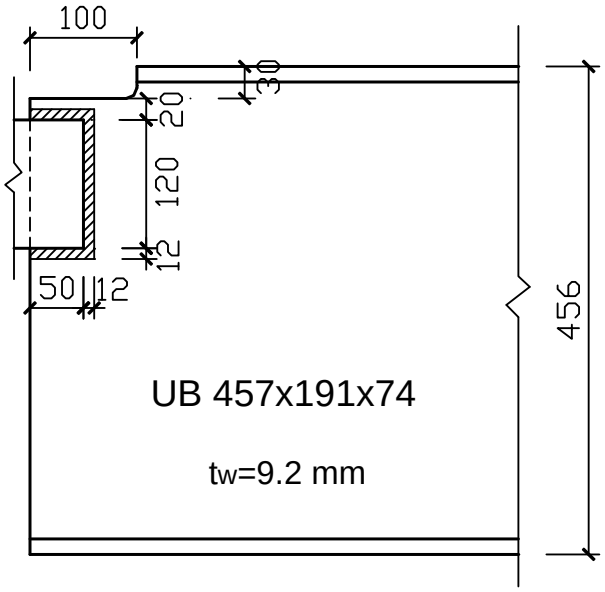


**Figure 24 Design example for the block shear of the coped beam with a welded clip angles connection**